NAVAL POSTGRADUATE SCHOOL
MONTEREY, CALIFORNIA

THESIS

AN INVESTIGATION OF SURFACE WAVES USING A TWO-AXIS SOURCE-RECEIVER COMBINATION

by

Anthony J. Anglin

June, 1996

Thesis Advisor: Anthony A. Atchley
Thesis Co-Advisor: Donald L. Walters

Approved for public release; distribution is unlimited.

REPORT DOCUMENTATION PAGE

Form Approved OMB No. 0704-0188

1. AGENCY USE ONLY *(Leave blank)*	2. REPORT DATE	3. REPORT TYPE AND DATES COVERED
	June 1996.	Master's Thesis

4. TITLE AND SUBTITLE TITLE OF THESIS. AN INVESTIGATION OF SURFACE WAVES USING A TWO-AXIS SOURCE-RECEIVER COMBINATION	5. FUNDING NUMBERS
6. AUTHOR(S) Anthony J. Anglin	
7. PERFORMING ORGANIZATION NAME(S) AND ADDRESS(ES) Naval Postgraduate School Monterey CA 93943-5000	8. PERFORMING ORGANIZATION REPORT NUMBER
9. SPONSORING/MONITORING AGENCY NAME(S) AND ADDRESS(ES)	10. SPONSORING/MONITORING AGENCY REPORT NUMBER

11. SUPPLEMENTARY NOTES The views expressed in this thesis are those of the author and do not reflect the official policy or position of the Department of Defense or the U.S. Government.

12a. DISTRIBUTION/AVAILABILITY STATEMENT Approved for public release; distribution is unlimited.	12b. DISTRIBUTION CODE

13. ABSTRACT

The goals of this thesis are 1) to design and test a two-axis surface wave source and two-axis surface wave receiver and 2) to investigate the use of surface waves to detect buried objects in water saturated sand. Results of measurements confirm the ability to generate particle motions in water saturated sand consistent with surface wave excitation. However, limitations in the size of the test tank prohibit a thorough investigation of the ability of the source and receiver to selectively excite and detect surface waves

14. SUBJECT TERMS Rayleigh waves; surface waves; mine detection	15. NUMBER OF PAGES 76
	16. PRICE CODE

17. SECURITY CLASSIFICATION OF REPORT	18. SECURITY CLASSIFICATION OF THIS PAGE	19. SECURITY CLASSIFICATION OF ABSTRACT	20. LIMITATION OF ABSTRACT
Unclassified	Unclassified	Unclassified	UL

NSN 7540-01-280-5500

Standard Form 298 (Rev. 2-89)
Prescribed by ANSI Std. 239-18 298-102

Approved for public release; distribution is unlimited.

AN INVESTIGATION OF SURFACE WAVES USING A TWO-AXIS SOURCE-RECEIVER COMBINATION

Anthony J. Anglin
Lieutenant, United States Navy
B.S., United States Naval Academy, 1990
Submitted in partial fulfillment
of the requirements for the degree of

MASTER OF SCIENCE IN ENGINEERING ACOUSTICS

from the

NAVAL POSTGRADUATE SCHOOL
June 1996

Author: _____
Anthony J. Anglin

Approved by: _____
Anthony A. Atchley, Thesis Advisor

_____
Donald L. Walters, Co-Thesis Advisor

_____
Anthony A. Atchley, Chairman
Engineering Acoustics Academic Committee

ABSTRACT

The goals of this thesis are 1) to design and test a two-axis surface wave source and two-axis surface wave receiver and 2) investigate surface waves to detect buried objects in water saturated sand. Results of measurements confirm the ability to generate particle motions in water saturated sand consistent with surface wave excitation. However, limitations in the size of the test tank prohibit a thorough investigation of the ability of the source and receiver to selectively excite and detect surface waves

TABLE OF CONTENTS

I. INTRODUCTION

A. OBJECTIVE

The purpose of this research was to design, build, and test a two-axis source and two-axis receiver to investigate the use of surface waves to detect buried objects in water saturated sand.

B. MOTIVATION

Previous research at the Naval Postgraduate School evaluated the feasibility of a phased array surface wave source to detect buried land/sea mines [Ref. 1]. The source and geophone combination used in that work were single-axis, constrained to vertical motions. That work demonstrated target localization using surface wave scattering, and beamforming with phased array techniques; however, the transmitted and received waves were not fully characterized. A logical progression of that research was to use a two-axis source and two-axis geophone combination to specifically excite and acquire surface waves. This two-axis source and two-axis geophone combination could then be used to investigate the feasibility of using elementary multi-axis signal analysis to enhance our understanding of surface wave propagation in water saturated sand. The purpose of this thesis was to build upon the results of the aforementioned research with a two-axis source and two-axis geophone combination. Similar techniques have been used by others [Ref. 2].

C. THESIS OUTLINE

The following topics will be discussed in this thesis:

1. Description of the test environment and data acquisition system.
2. Design and calibration of the two-axis geophone.
3. Design and characterization of the two-axis source.
4. Comparison the single-axis source/two-axis geophone combination to the two-axis source/two-axis geophone combination.
5. Investigation of the feasibility of using polarization filtering and Cepstrum analysis with the single-axis source/two-axis geophone combination and the two-axis source/two-axis geophone combinations to detect buried objects in water saturated sand.

II. APPARATUS

The purpose of this chapter is to 1) describe the test tank, 1) describe the LABVIEW data acquisition system, 3) describe the design and calibration the two-axis geophone, and 4) describe the design of the two-axis source.

A. TEST TANK

All of the experiments associated with this thesis were conducted in a round, 1.8 radius, 1.2 m deep redwood tank. The tank's redwood bottom covers a hard cement laboratory floor. This tank was filled with approximately 17 tons of medium grain (0.6 mm) beach sand from Moss Landing in Monterey County, California [Ref. 1]. There was a 3.7 m x 5 cm x 3.2 cm aluminum beam mounted 10 cm above the sand. This beam was used to mount the source above the sand (see Fig. 2.1). The tank was conditioned prior to each experiment. This conditioning included uniformly wetting the surface with a garden hose with spray attachment, and uniformly pounding the surface of the sand with a 50 cm x 50 cm square board attached to a wooden pole to ensure uniform packing of the grains near the surface.

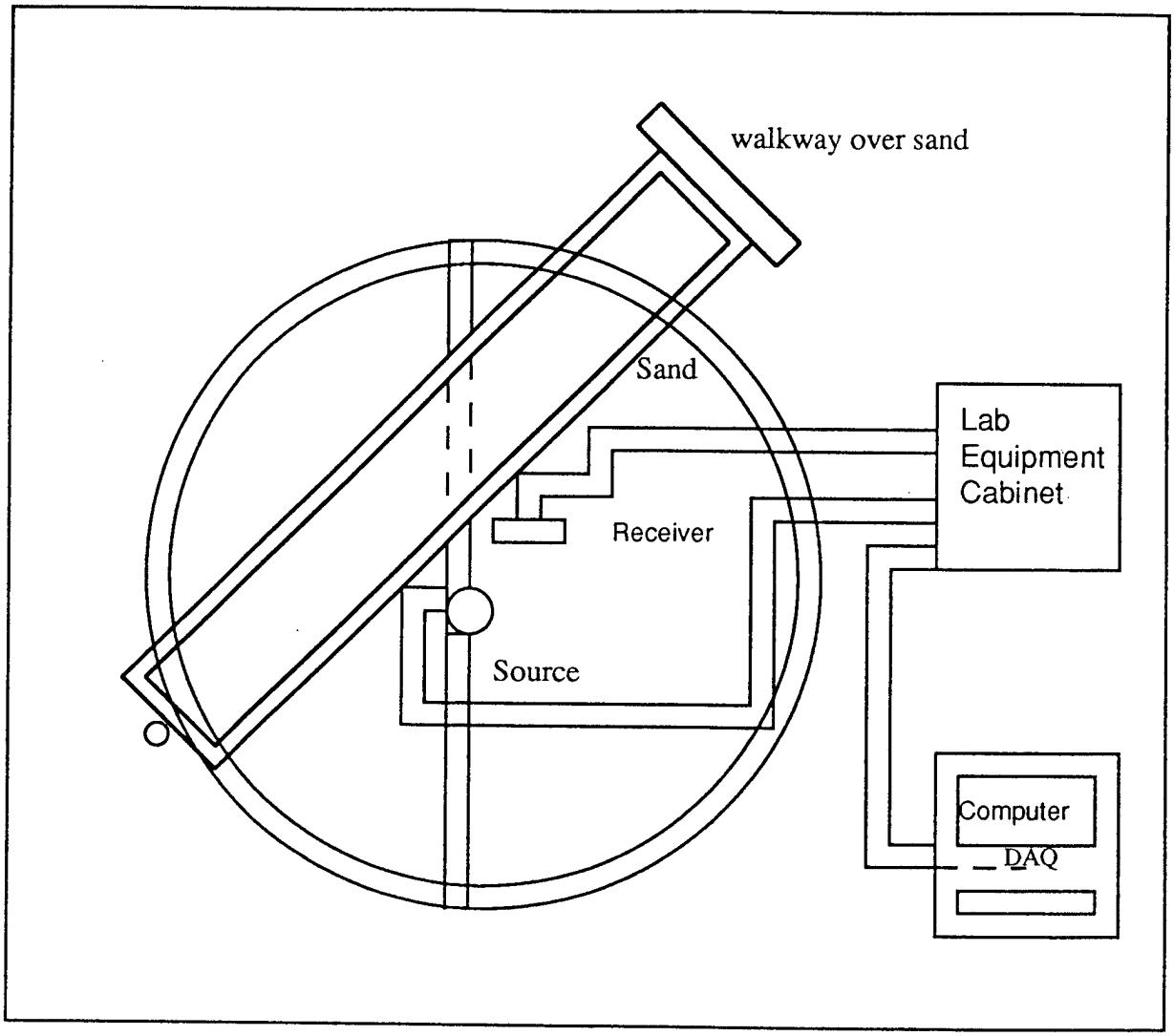

Figure 2.1 Diagram showing top view of the water saturated sand-filled redwood test tank. The two lines leading to/from the source and receiver emphasize that both are two-axis devices.

B. DATA ACQUISITION SYSTEM

Most of the data acquisition associated with this thesis was performed with LABVIEW version 3.1.1. A product of National Instruments Corporation, it is a graphical, general-purpose programming language with extensive libraries of functions, an integral compiler and debugger, and an application builder for stand-alone applications [Ref. 3]. In addition to the software, three plug-in boards were utilized: the NB-MIO-16XL Data Acquisition board, the NB-AO-6 Analog Output board and the NB-DMA-2800 Direct Memory Access board. The LABVIEW software was used on a Power Computing model 100 computer (see Appendix A). Source code for post-acquisition processing was written using MATLAB 4.2.

C. TWO - AXIS GEOPHONE DESIGN PARAMETERS

As in Ref. 1, the design requirements for the two-axis geophone to detect vibrations in the sand were the following:

1. It should have adequate sensitivity to ground motion generated by the source within the ranges provided by the tank.

2. It should have adequate sensitivity in the frequency band of interest, nominally 200 to 400 Hz.

3. It should have good coupling to the sand that could give repeatable results.

Additional requirements for this thesis were:

4. It should be capable of sensing both vertical and horizontal components of the signals.

Figure 2.2 shows a diagram of the two-axis geophone. The sensors are Applied Magnetics Geo Space model number HS-1 miniature geophones (see data sheet in Appendix B). The two-axis geophone housing is made of machined aluminum. The vertical geophone is secured to the housing by a threaded rod manufactured into the geophone case. The horizontal geophone is secured by set screws in the aluminum housing. The 5.2 cm sand 'coupling peg' was the same coupler used on the model S4408A sensors used in Ref. 1.

D. TWO-AXIS GEOPHONE CALIBRATION

The two axis geophone was calibrated using a HP3562A Dynamic Signal Analyzer, (APS) Acoustic Power Systems Inc. Dual Power Amplifier, APS Model 1201 Perma-Dyne Shaker Table, and a calibrated model J353B03 PCB Piezotronics Accelerometer. The horizontal axis geophone was calibrated by mounting the shaker horizontally on a stable base. The geophone and accelerometer were securely mounted on the shaker table with a specially manufactured mounting plate. They were mounted with their sensitive axis aligned horizontal. The swept sine output from the HP 3562A was amplified by the APS Dual Power amplifier and applied to the shaker table. The frequency

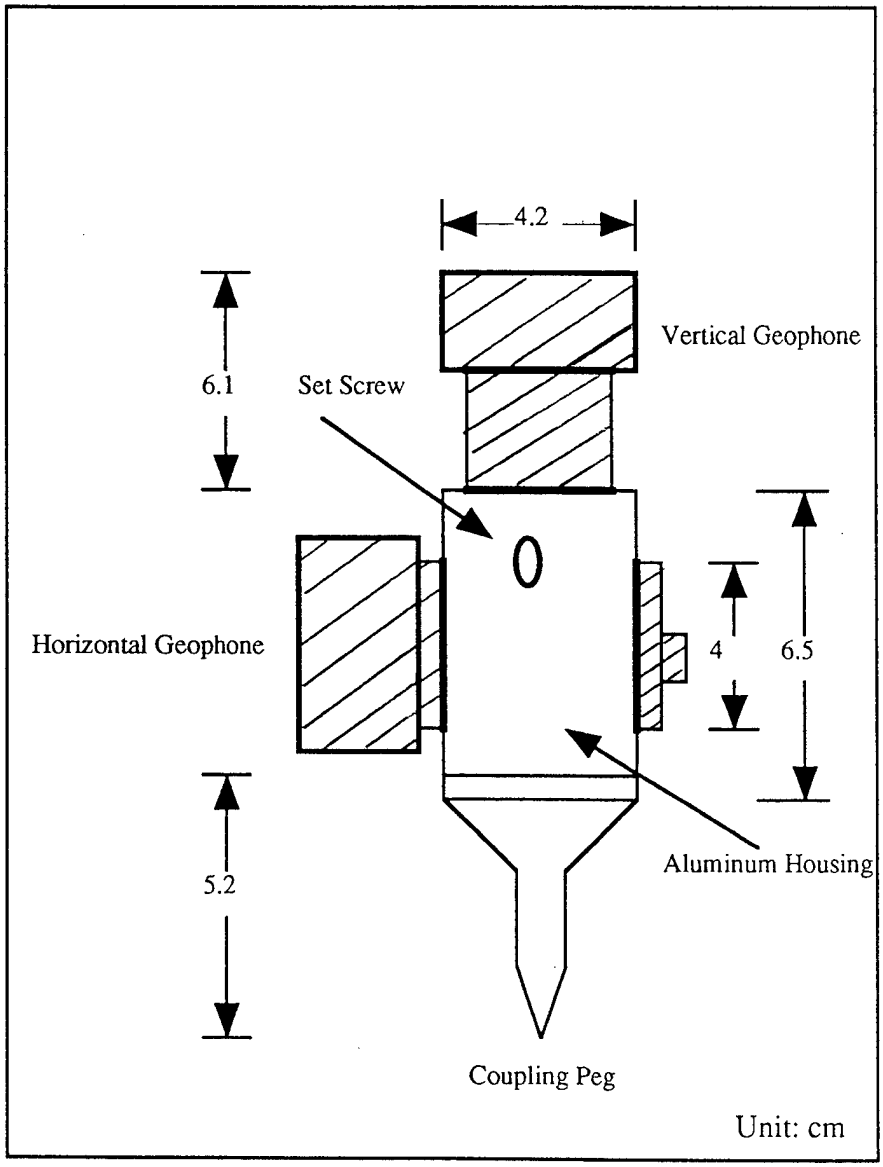

Figure 2.2. Diagram showing the design of the two-axis geophone. The hatched portions indicate the individual single-axis geophones mounted in an (unhatched) aluminum block.

range of the sweep was 0-1000 Hz. The resultant accelerometer and geophone responses were applied to channels one and two of the dynamic signal analyzer. The built-in frequency response was used to determine the frequency response from these signals. Data was read from the display, using cursors, in 20 Hz increments and entered into a Matlab file. The calibration curve shown in Fig. 2.3 was computed in the following manner. The velocity of the accelerometer must equal that of the geophone

$$u_a = u_g. \tag{2.1}$$

The velocity is related to acceleration by $u = a/\omega$. The sensitivity of the accelerometer S_a is given in mV/g, where $g = 9.81\ m/s^2$. The voltage output of the accelerometer V_a is converted to a velocity according to

$$u_a = (9.8\ m/s^2/g)\ (V_a/S_a\omega), \tag{2.2}$$

where V_a is in mV. The voltage output of the geophone is converted to velocity according to

$$u_g = V_g/S_g \tag{2.3}$$

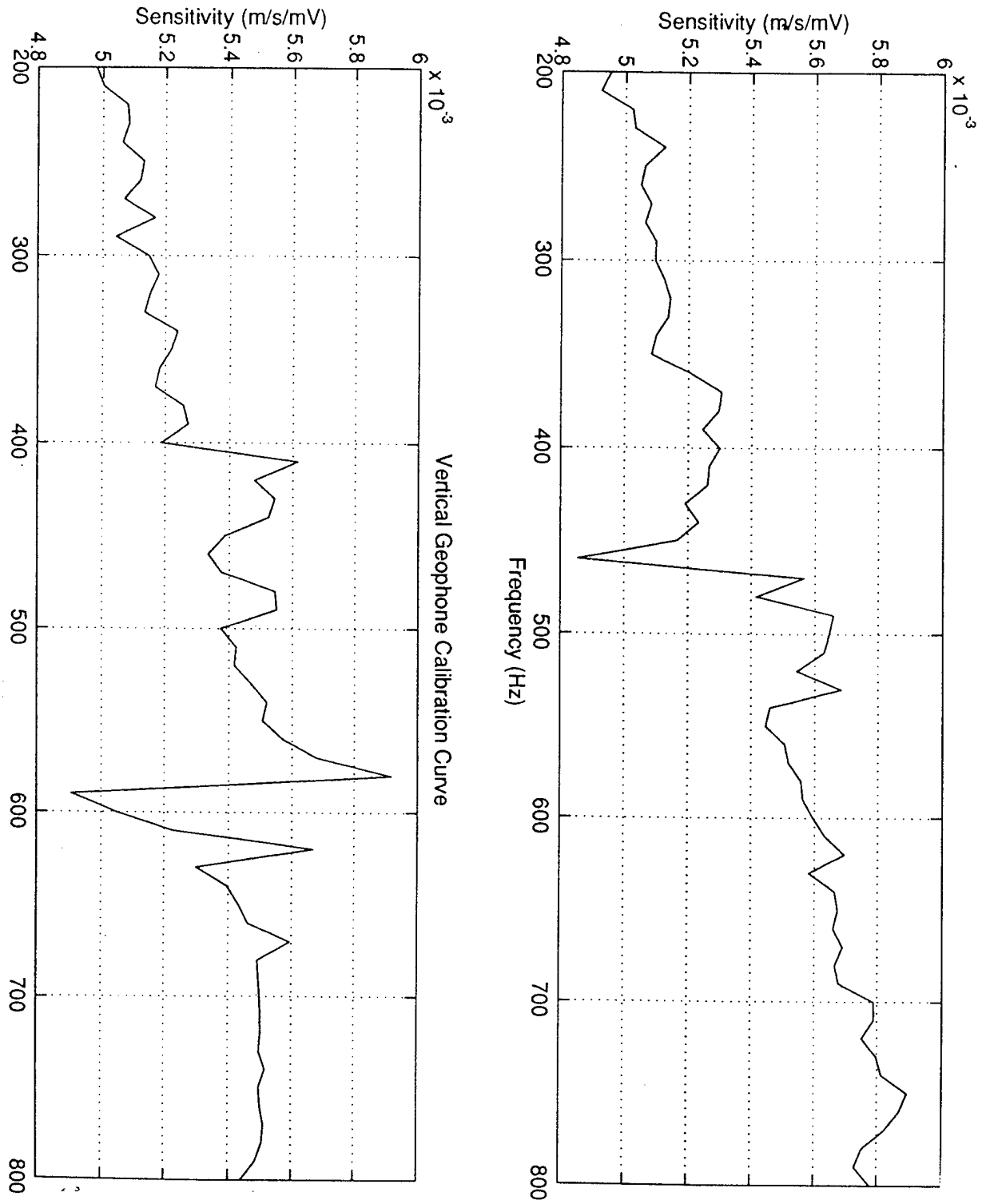

Figure 2.3. Calibration curves for the horizontal (top) and vertical (bottom) geophones.

where V_g is in mV and S_g is the sensitivity of the geophone in mV/m/s. Setting the two velocities equal and solving for S_g gives

$$S_g = (V_g/V_a)(\omega/9.81 m/s^2/g)S_a. \quad (2.4)$$

The vertical axis geophone was calibrated in the same manner except the shaker was mounted vertically.

As can be seen from Figs. 2.3a and b the vertical and horizontal calibration curves are similar over our anticipated operating frequency range. Therefore for comparison purposes, equal voltages from the two geophones correspond to approximately equal velocities. In the results presented later, the output voltages will be used rather than velocities.

E. TWO - AXIS SOURCE DESIGN PARAMETERS

The two-axis source design was guided by some of the same requirements as in Ref. 1:

1. It should generate signals with sufficient amplitude to allow detection of the surface waves anywhere in the test tank.

2. It should provide a repeatable waveform.

3. It should be capable of a wide range of repetition rates.

4. It should have good ground coupling that would last for an extended period.

5. It should provide clean signals over a range of frequencies from approximately 200-400 Hz.

The focus of this thesis required the following design criteria:

6. It should be capable of generating two-axis motion.

7. It should be portable and capable of being quickly moved and reset in order to facilitate conducting experiments of various source/geophone configurations in relatively short periods.

Figure 2.4 shows the final design. Two four inch diameter model 4A9, high cone excursion, electrodynamic speakers were mounted at right angles to one another on an aluminum support plate (see data sheet in Appendix C). Connecting rods coupled the drivers to a 7.3 sq. cm source foot. The 7.5 cm rods were attached to the foot with machined holes and set screws. The mounting block's dimensions were 2.5 cm x 1.0 cm x 0.75 cm. The block was epoxied to the foot. The foot consisted of an array of 25, 4 cm long nails mounted on a 2.7 cm x 2.7 cm brass plate and arranged in a square pattern, spaced by 0.6 cm to improve contact with the sand. The 7.5 cm rods were attached to the speaker cones by threaded aluminum caps that were epoxied to the speaker cones.

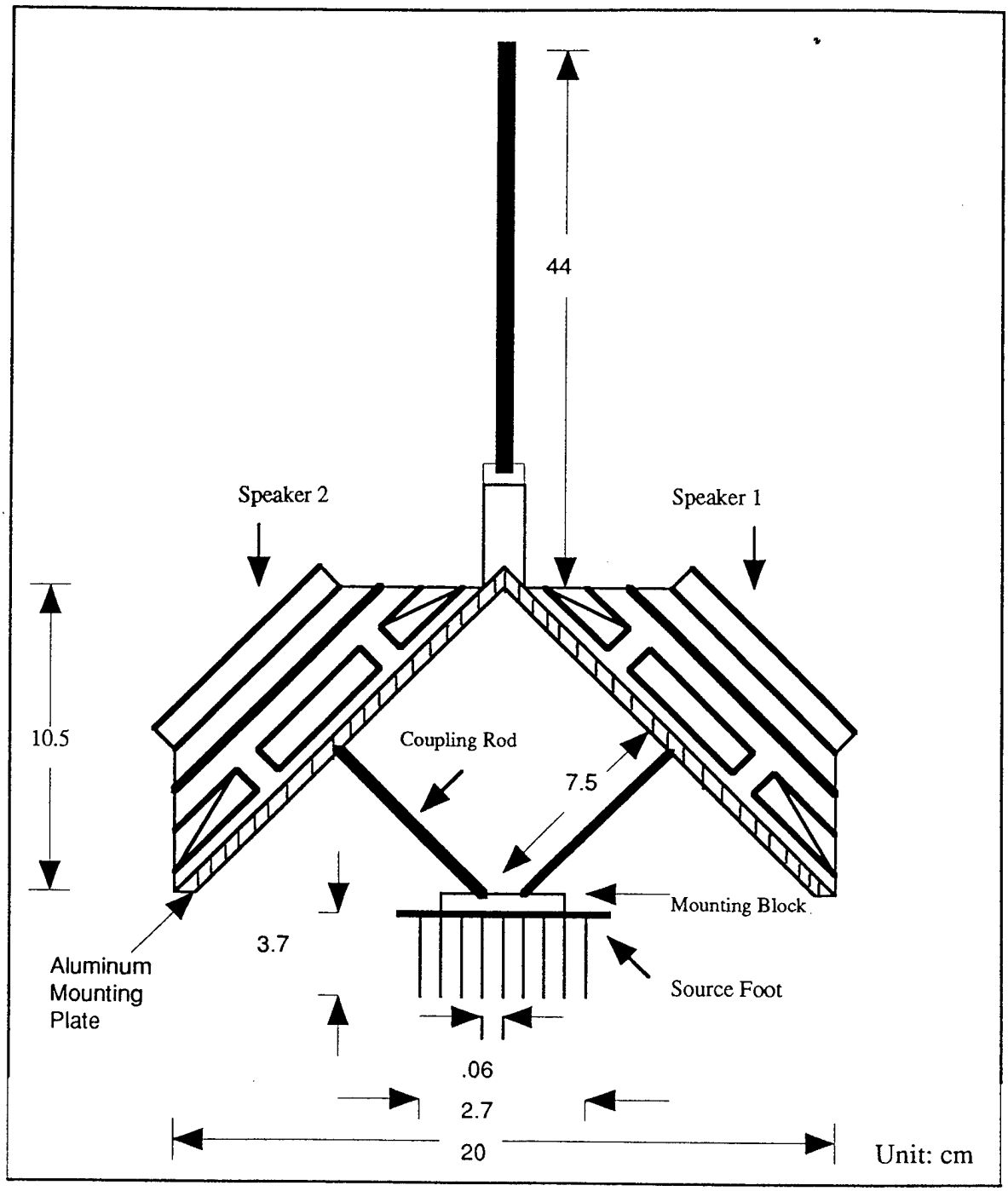

Figure 2.4. Diagram showing the design of the two-axis source. The two electrodynamic loud-speakers are mounted at a right angle. Two connector rods transfer the speaker's diaphragm motion to the "bed of nails" foot.

F. SUPPORTING EQUIPMENT

The typical experimental arrangement is shown schematically in Fig. 2.5. The two-axis source was driven by the outputs of two HP3314A function generators, each amplified by one channel of a Techron model 5507 power amplifier. One HP 3314A was triggered by the other, so that the relative phases of the outputs could be adjusted.

The two geophone outputs were sent to bandpass filter-preamplifiers (one Stanford SR 560 and one Ithaco 1202). The outputs were sent to an oscilloscope and the A/D boards.

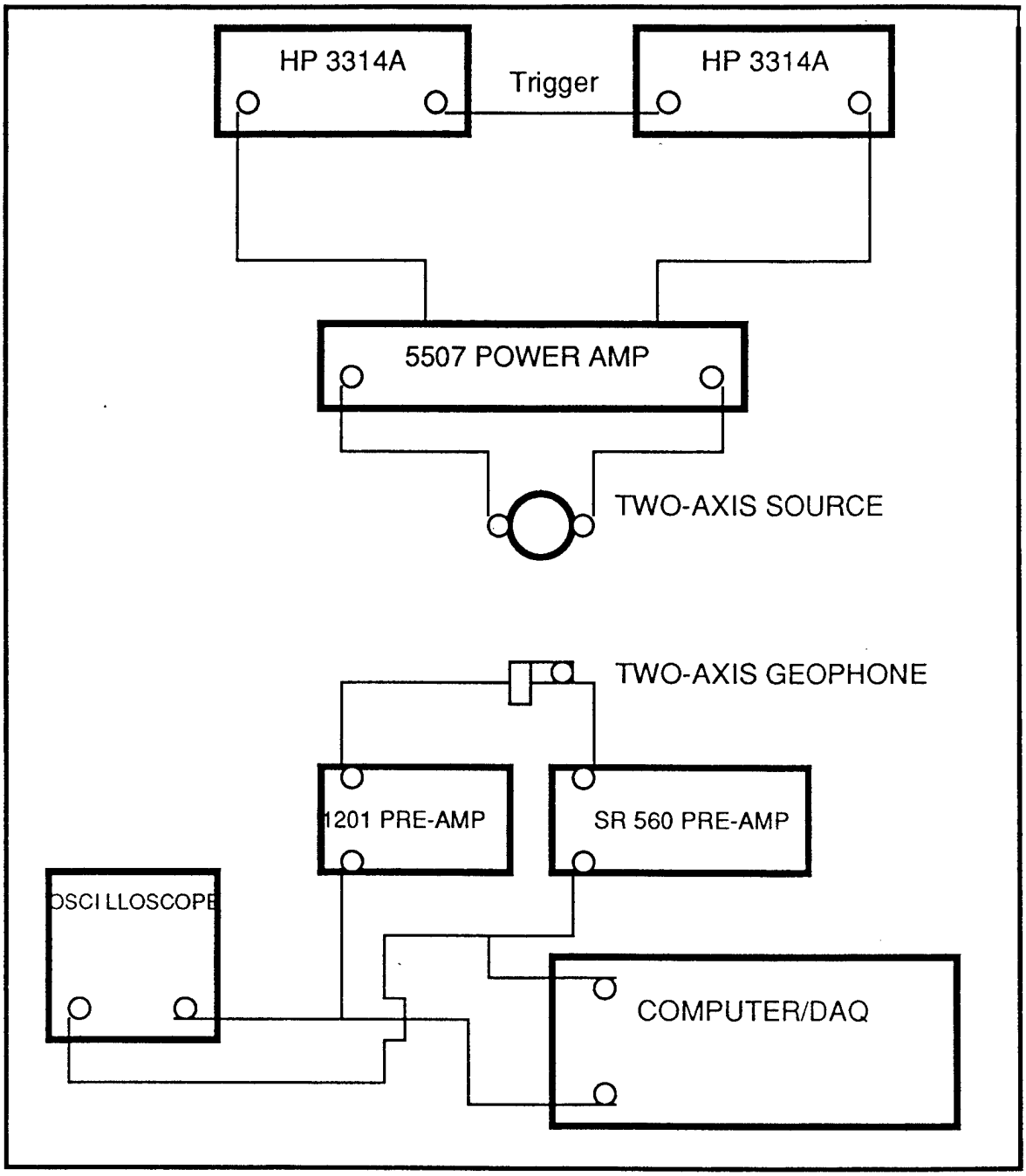

Figure 2.5. Block diagram showing the typical electrical equipment used in the measurements. The relative phases of the outputs of the two function generators can be adjusted over the range -180 to 180^0.

III. TWO-AXIS SOURCE CHARACTERIZATION

The purpose of this chapter is to 1) describe the characterization of the two-axis source, 2) investigate frequency dependent attenuation in the test environment, and 3) use polarization filtering to further investigate the ability of the two-axis source to excite surface waves.

A. TWO-AXIS SOURCE CHARACTERIZATION

Two PCB model 303A03 miniature accelerometers were mounted vertically and horizontally on the foot of the two-axis source. The source was driven with a 50 cycle, 400 Hz pulse with pulse repetition frequency of 1 Hz. The phase relationship between the drive signals was varied and the resultant source-foot vibrations were sensed by the accelerometers and acquired with LABVIEW. This experiment was repeated for two conditions; for the foot in air and for the foot coupled to the sand. Signals were also acquired from the two-axis geophone at a range of 20 cm from the source. The vertical signals were plotted versus the horizontal signals in order to compare the in-air accelerometer signals, the in-sand accelerometer signals and the received two-axis geophone signals.

Figures 3.1 and 3.2 show a series of plots of the in-air and the in-sand accelerometer signals for different phase relations. The notation 'Rm5L90' indicates that the right channel was driven by a signal with phase minus five degrees and the left channel

was driven by a signal with a phase of positive 90 degrees. The other plot labels can be interpreted in the same manner. These x-y patterns show that the two-axis source motion can be manipulated to produce a range of foot motions for various drive phases. The sand motion detected by the two-axis geophone is depicted in Fig. 3.3. The geophone signals were dominated by vertical motion. Although it was not possible to generate purely horizontal motion, it was possible to introduce a phase shift between vertical and horizontal motions. The reason for the relative lack of horizontal motion control is not clear. It may be due to restrictions of the foot motion by the sand or the connecting rods, or it may be due to some more fundamental limit. The foot is more free to move vertically. However, Fig. 3.3 shows that it is possible to generate near-elliptic motion in the sand.

The motion of the sand as detected by the two-axis geophone is also dependent on the relative azmuthal location of the geophone with respect to the source. Figure 3.4 shows the resultant patterns from signals received at 0, 90, 180, and 270 degrees relative to the source at a range of 20 cm from the source. The 0^0 reference was a line perpendicular to the plane containing the connecting rods (see Fig. 3.5). As the geophone was moved from location to location the horizontal axis was pointed in a direction parallel to the connecting rod plane. All subsequent experiments were conducted with the geophone in the 90^0 orientation.

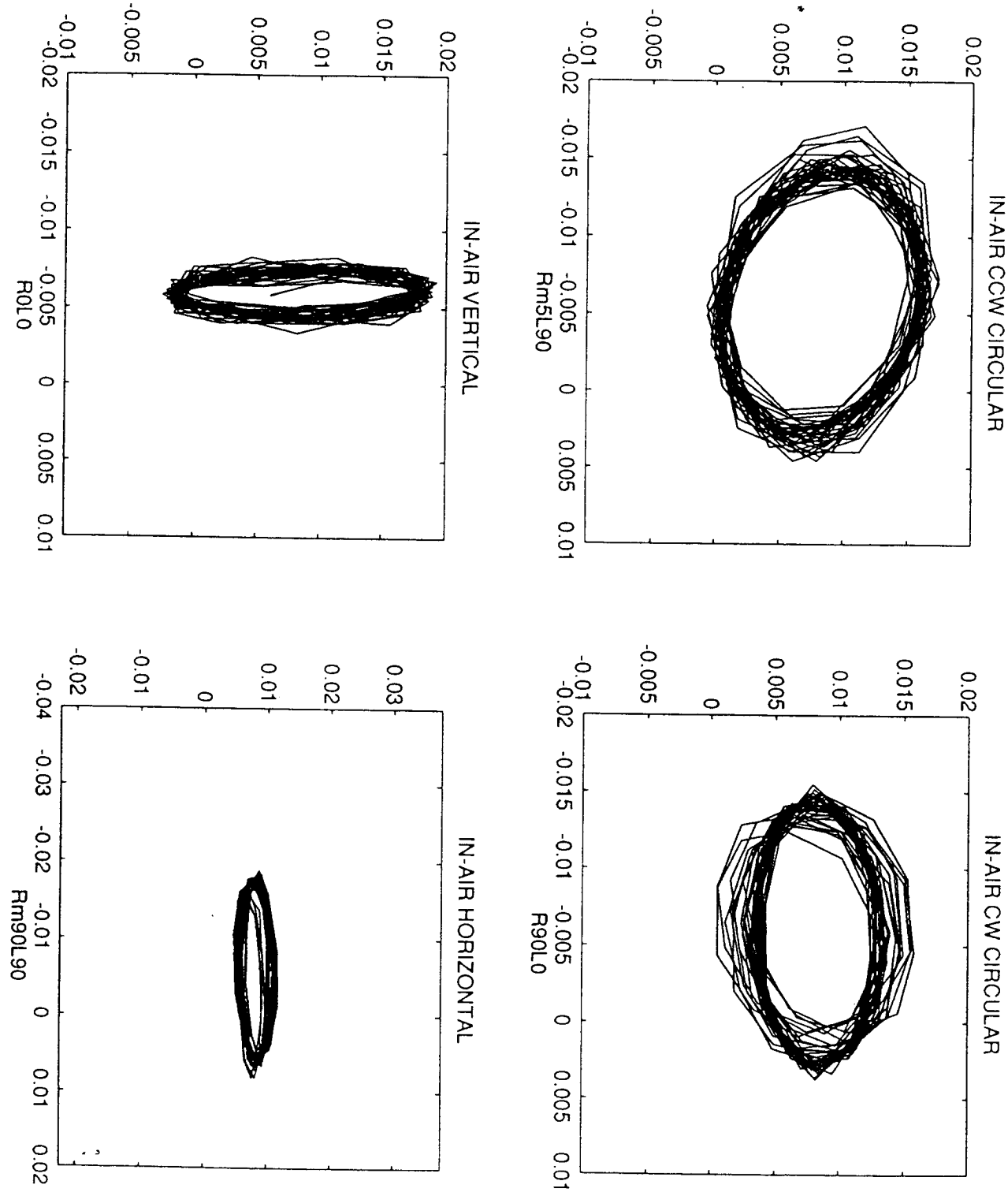

Figure 3.1. Plots showing the motion of the foot in air. The graphs show the output of the vertical accelerometer versus the output of the horizontal accelerometer for the four different phase conditions applied to the two-axis source.

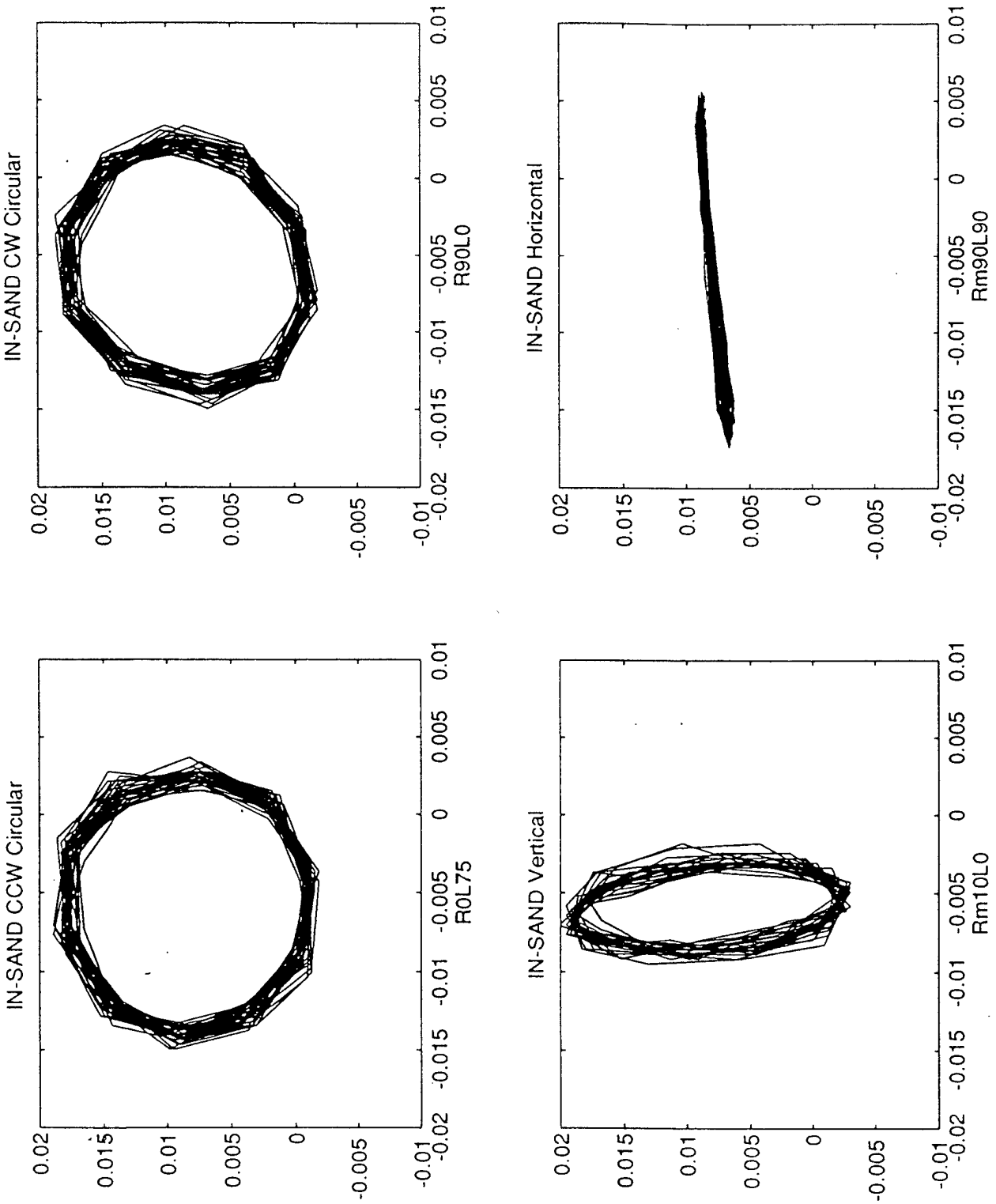

Figure 3.2. Same as Figure 3.1, except the foot is coupled to the sand.

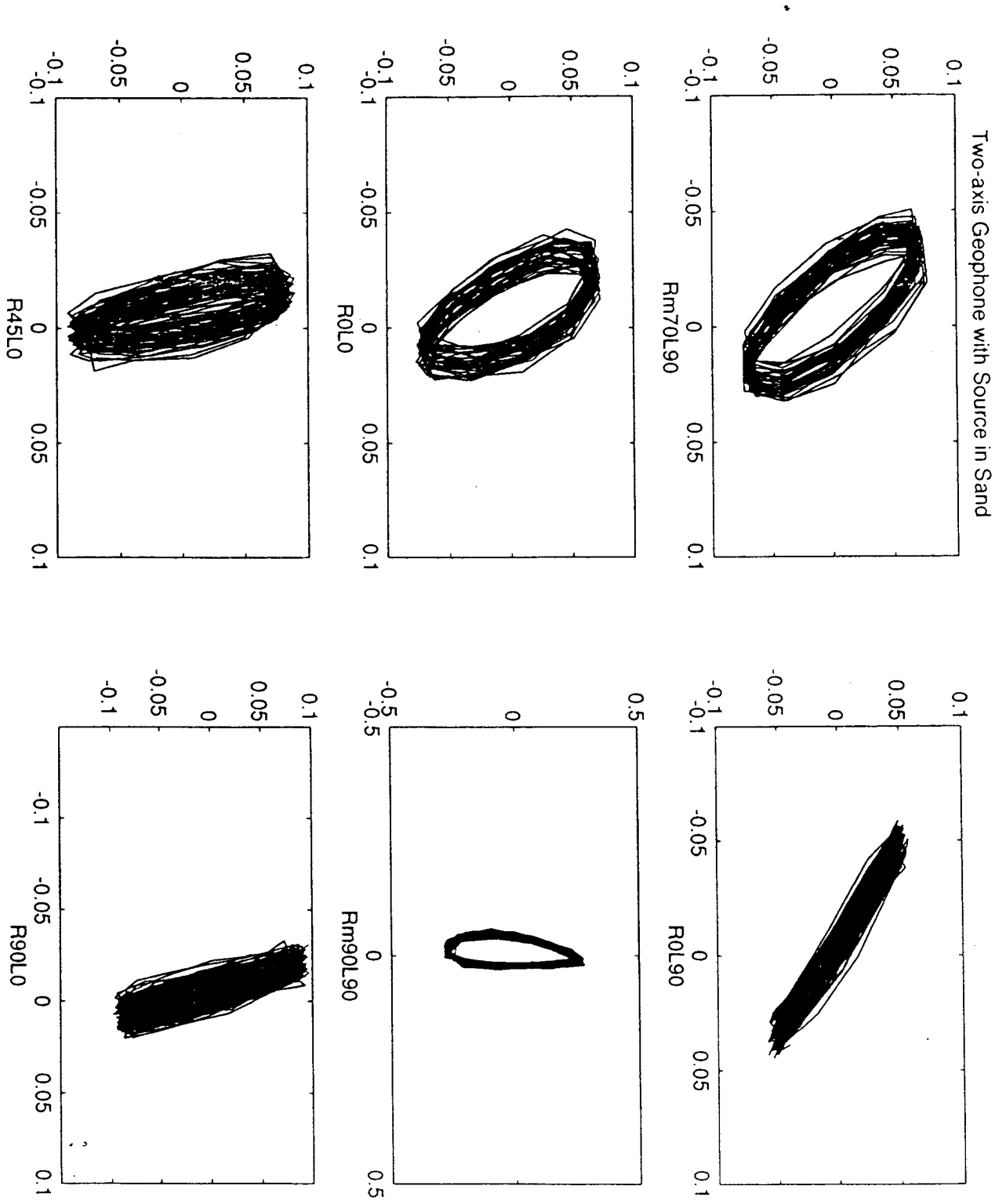

Figure 3.3. Plots of the output of the vertical geophone versus the output of the horizontal geophone for various drive phases.

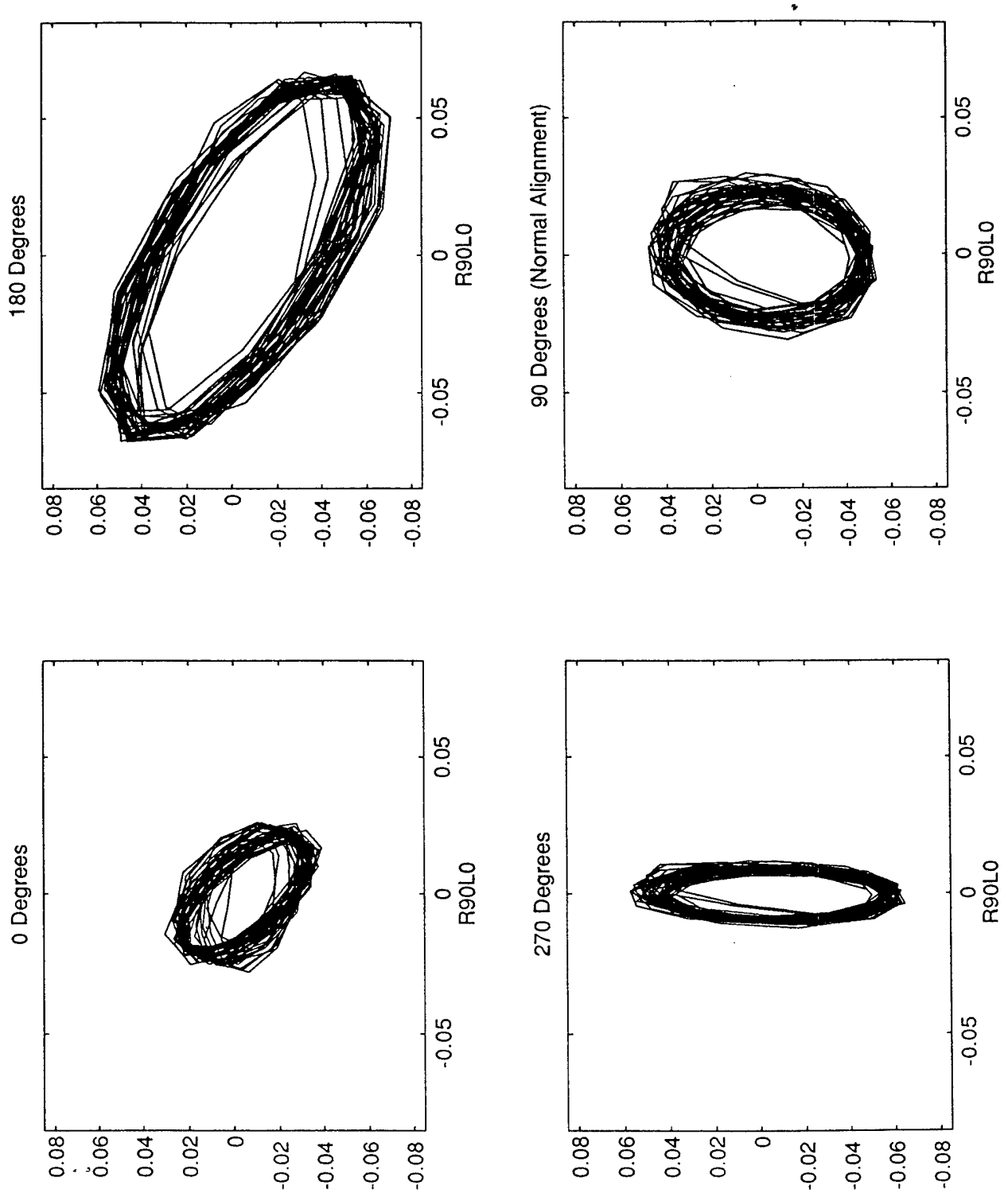

Figure 3.4. Plots of the sand motion detected by the geophone for four different azmuthal orientations of the geophone relative to the source. The orientations are define in Fig. 3.5.

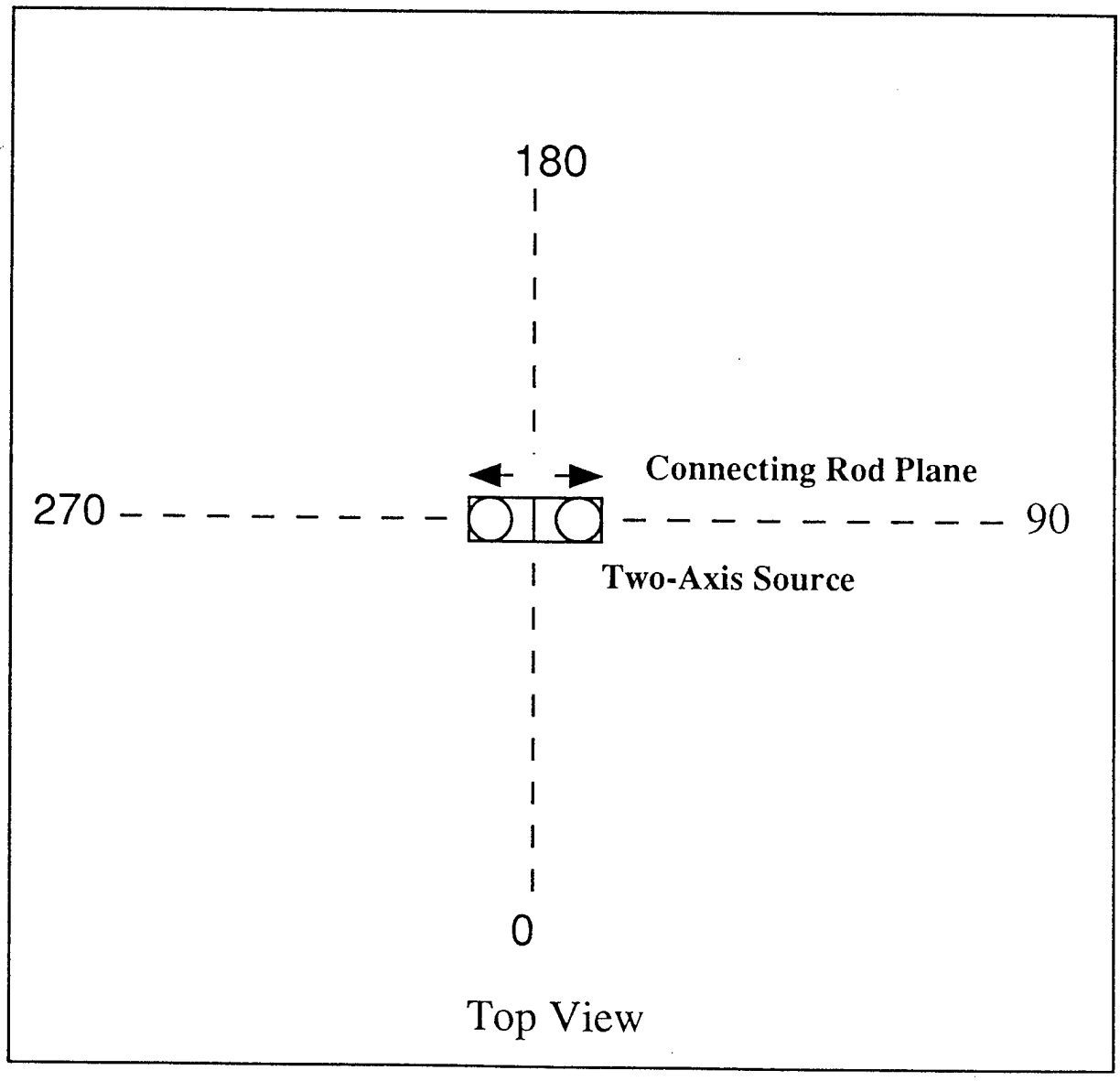

Figure 3.5. Top view showing how the azmuthal orientations used in Fig. 3.4 are defined.

B. RANGE DEPENDENCE OF SIGNALS

Figure 3.6 shows two representative vertical and horizontal geophone signals measured at a range of 20 cm from the source. The two-axis source was driven with single-cycle, 90 degree phase shifted, 400 Hz signals with a 1 Hz repetition frequency. The data shown in Fig. 3.6 show a number of the features. First, the response in the sand was not a single cycle. Also the vertical and horizontal signals are very different. There is evidence of multiple arrivals, especially in the horizontal signal. The structure of the received signal is very range dependent. In an effort to demonstrate this, the waveform amplitude corresponding to the feature pointed out in Fig. 3.6, was plotted vs. range for signals in the frequency range 200 to 800 Hz and ranges 20 to 120 cm from the source. Figure 3.7 shows the results for frequencies 200, 400, and 600 Hz. The expected consistent monotonic decrease in amplitude with range was not observed. Instead, the irregular amplitude variations with range indicate that this tank does not model free field conditions. We decided to use 400 Hz for further investigation.

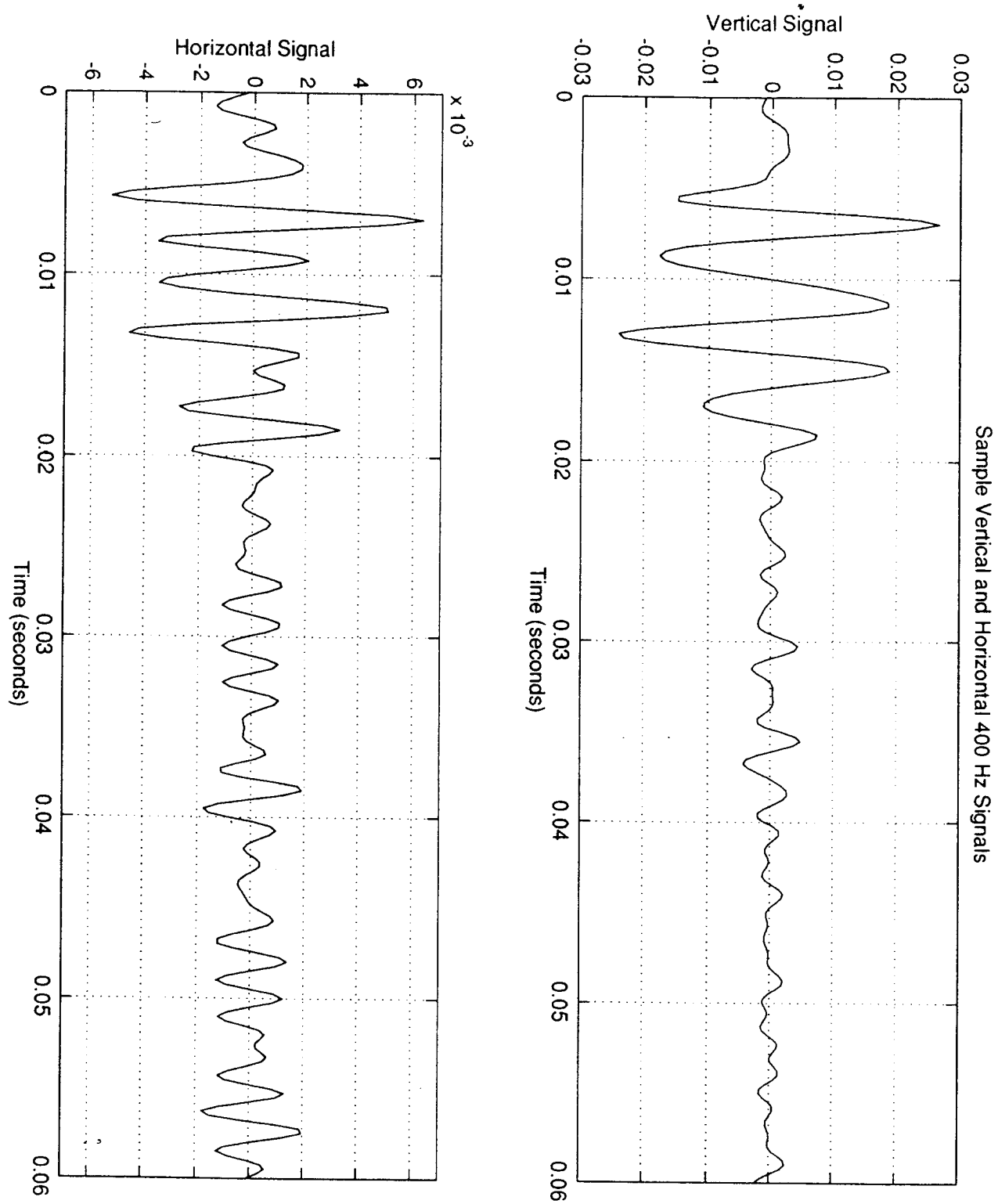

Figure 3.6. Graphs of the output of the vertical (top) and horizontal (bottom) geophones as functions of time. The source was driven in phase with a single 400 Hz cycle.

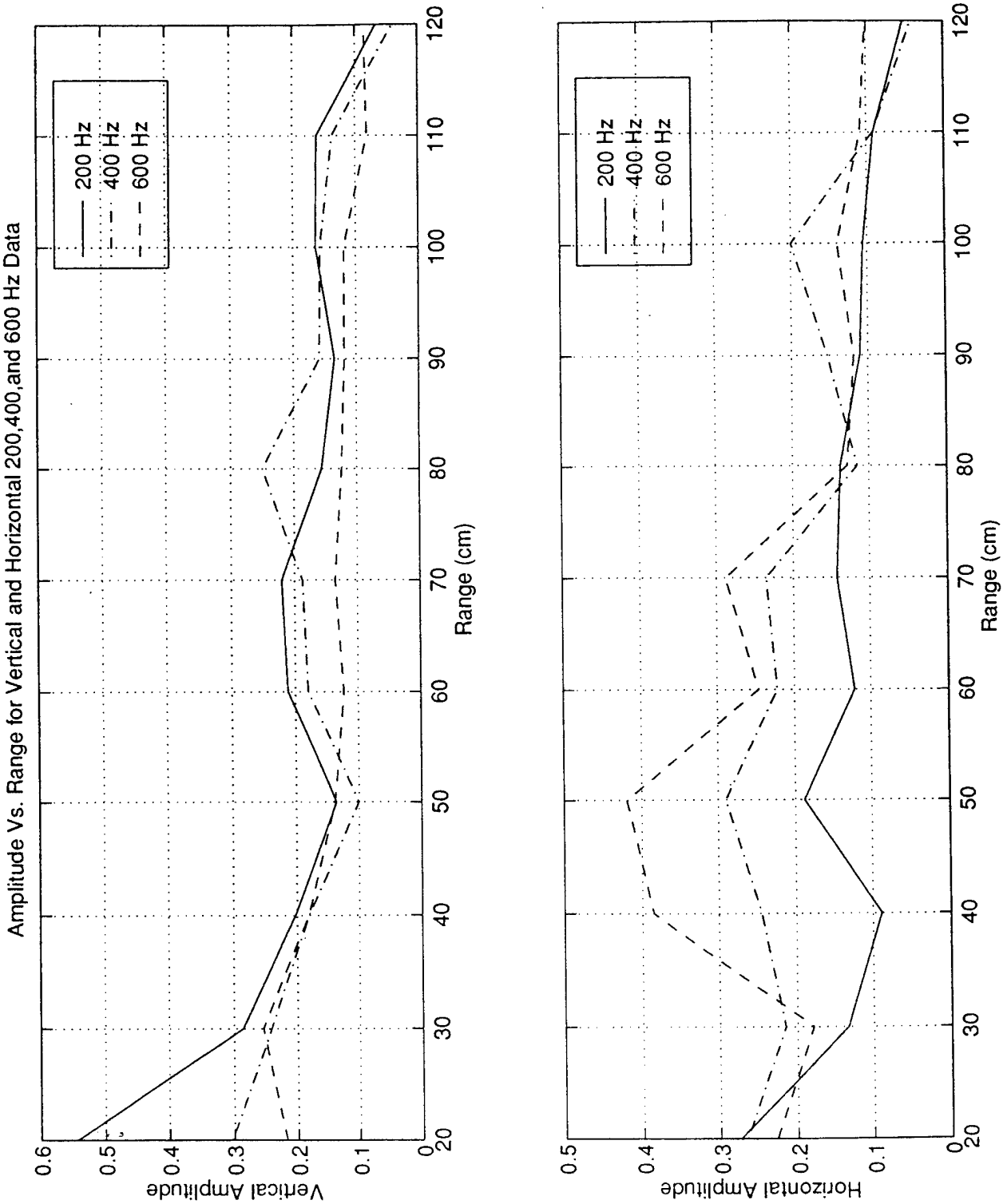

Figure 3.7. Plots of the amplitude of the vertical (top) and horizontal (bottom) geophones as functions of range for 200, 400, and 600 Hz drive frequencies.

C. POLARIZATION FILTERING

One way to detect surface waves in the presence of other modes of propagation (such as compressional and shear) is to use polarization filtering. As described in Ref. 2, the function of the polarization filter is to make use of the horizontal/vertical phase offsets characteristic of surface waves to preferentially extract surface wave signatures but reject signals due to other propagation modes.

The first step in the analysis was to convert the real horizontal signal x(t) into a complex analytic signal X(t). X(t) is defined as

$$X(t) = x(t) + jx'(t), \tag{3.1}$$

where x'(t) is the Hilbert transform of x(t) defined through

$$x'(t) = 1/\pi\int x(t)/(t-\tau)d\tau. \tag{3.2}$$

The vertical signal was similarly converted to an analytic signal Y(t). For monofrequency signals, the two functions X(t) and Y(t) should differ by a constant phase angle, characteristic of surface waves. The product $X^*(t)Y(t)$, were * denotes the complex conjugate, yields a complex term whose imaginary part is sensitive to the phase difference between the two signals. $Im[X^*(t)Y(t)]$ is zero if x(t) and y(t) are in phase; it is nonzero

otherwise. If the phase is such that the particle motion is prograde (retrograde) the imaginary part is positive (negative).

To test this technique, this analysis was performed on two sets of computer generated waveforms. Figures 3.8 and 3.9 show the results. In the upper trace of Fig. 3.8, there are two waveforms (solid and dashed) that consists of two gaussian shaped pulses. The frequency of the signals in each of the pulses is 400 Hz. The relative phase between the first pulses of the two signals is 90^0. The second pulses are in phase with each other. The lower trace shows the results when this analysis was performed on the signals in the upper trace. Note that the in-phase portions (the second pulses) of the signals were eliminated. The out of phase portions result in an envelope with period proportional to the period of the two out-of-phase (first pulses) signal portions. Figure 3.9 shows the results of polarization analysis on signals similar to the signals in Fig. 3.8. The only difference is the relative phase of the first pulses is 270^0 (-90^0). Note that the 90^0 shift results in a positive output, while the -90^0 shift results in a negative output.

When this algorithm was applied to a set of received horizontal and vertical signals as in Fig. 3.6 the results were very different from the theoretical results. This lead to a re-examination of the received signals. Upon further review, a difference was observed in the received vertical and horizontal signal's frequency. This frequency difference is evident upon careful review of Fig. 3.6. Apparently the two-axis source has different frequency and phase responses in the vertical and horizontal directions. Because there is no

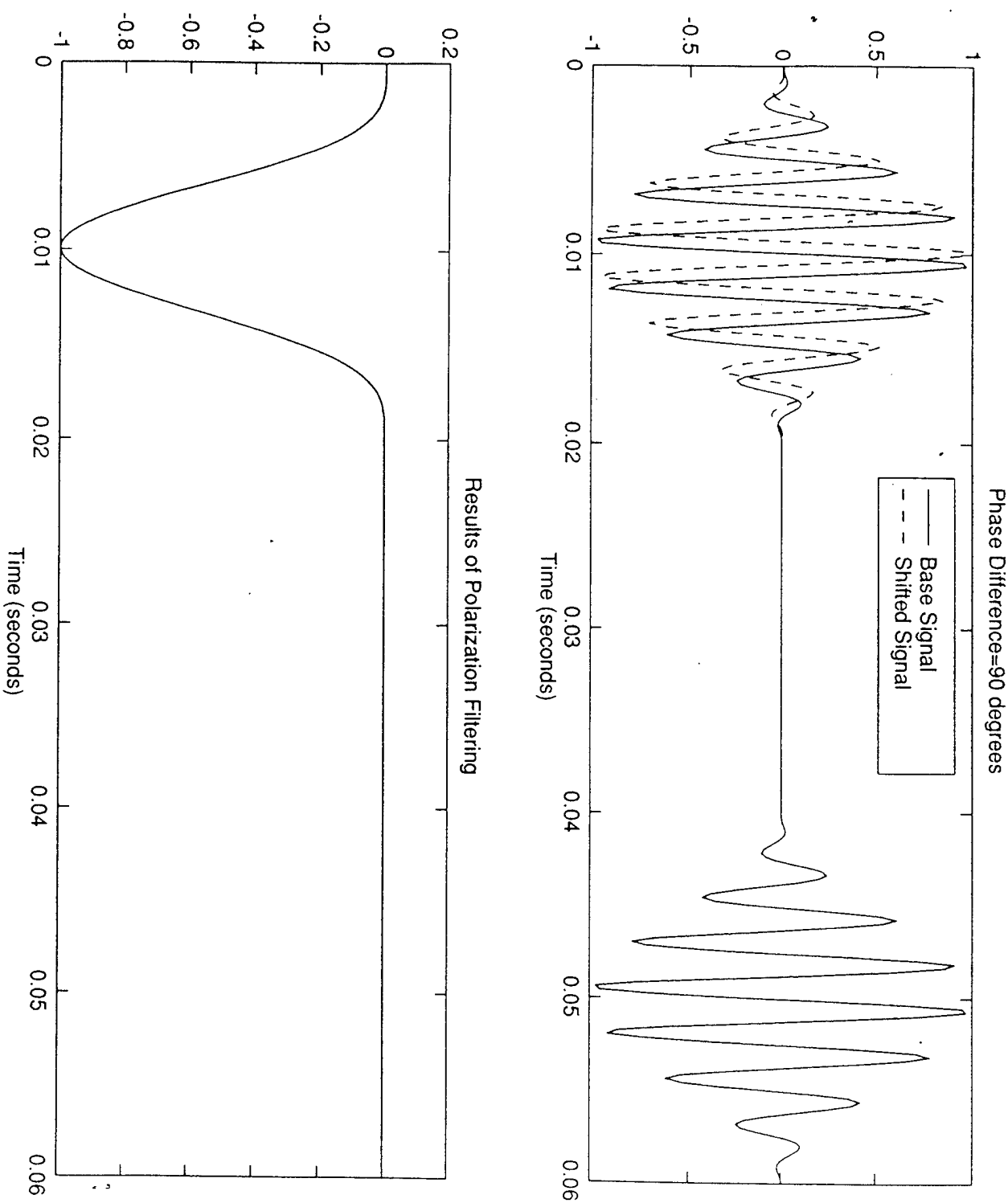

Figure 3.8. Graphs showing computer generated signals (top) used to test Polarization filtering, an algorithm that uses a Hilbert transform technique to detecting a phase shift between two signals. The results of the polarization filtering technique is shown in the bottom graph.

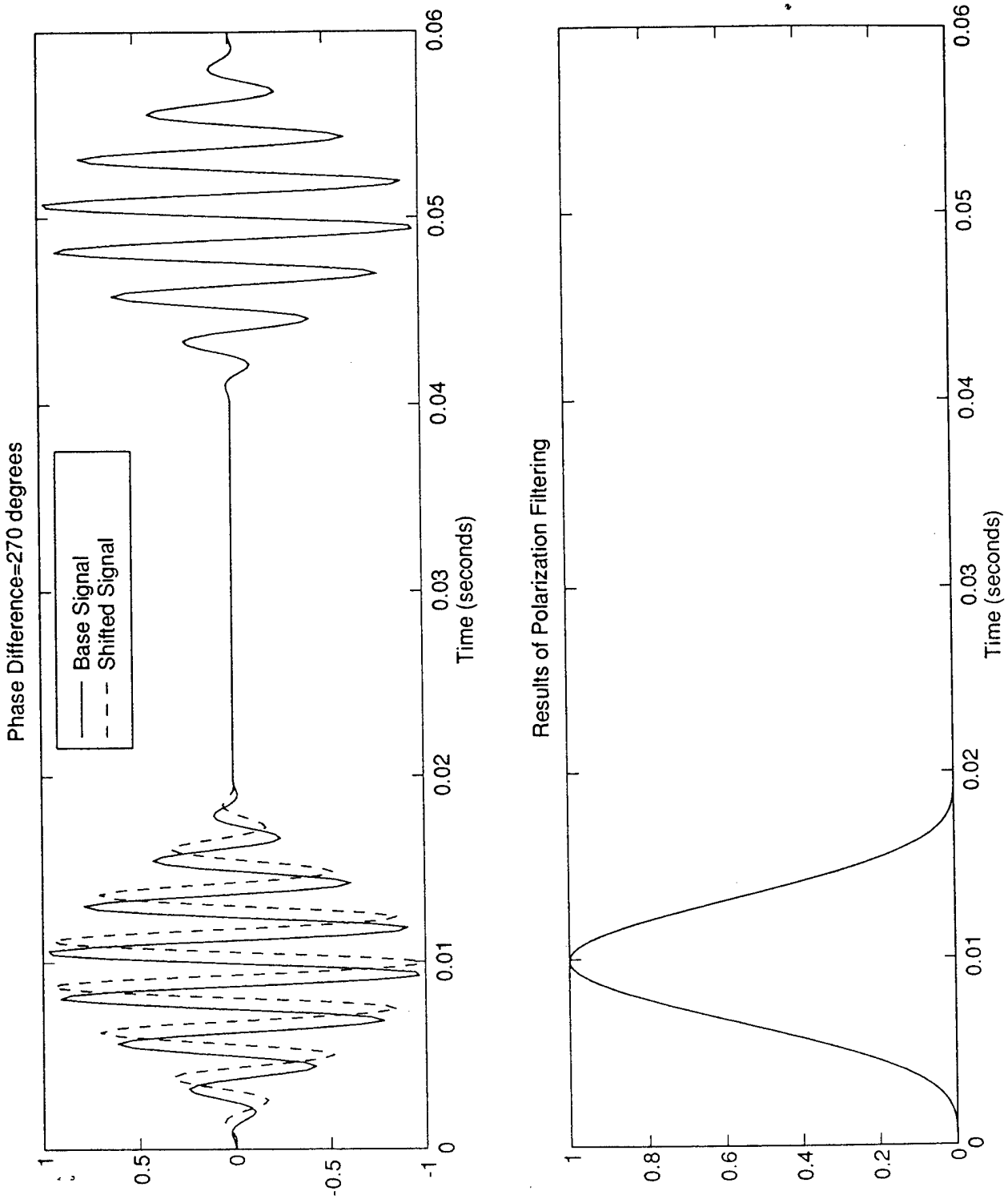

Figure 3.9. Same as Fig. 3.8 except the phase difference between the signals in the first pulse is 270^0 rather than 90^0 as in Fig. 3.8. The output of the polarization filter is opposite in sign to the one in Fig. 3.8.

consistent phase relationship between frequencies of two different frequencies, polarization filtering cannot be used to detect surface waves.

To demonstrate this problem, polarization analysis was performed on the two dual-envelope signals shown in Fig. 3.10. The upper trace shows two computer generated signals. The dashed signal consists of two gaussian envelopes. The frequency of the signal in the first envelope is 300 Hz and the frequency of the signal in the second envelope is 400 Hz. The solid line signal also consists of two gaussian shaped pulses. The frequency of the signals in each of the pulses was 400 Hz. The lower trace of Fig. 3.10 shows the results of applying this algorithm on these computer generated signals. One can see that polarization filtering gives a bipolar output for these signals. Figure 3.11 shows a comparison of the results of polarization analysis on the computer generated signals in Fig. 3.10 and the real acquired signals. These signals are very similar. These results seemed to indicate that the polarization analysis conducted on the real signals revealed different frequencies in the received vertical and horizontal signals.

The problem of two different frequency responses can be overcome by driving the source long enough to reach steady state. This is demonstrated in the next sequence of figures. Figure 3.12 shows the outputs of the vertical and horizontal accelerometers mounted on the foot for two different drive conditions, 1 cycle and 10 cycles. As might be expected, the accelerometer outputs for the 1 cycle drive roughly resemble decaying oscillations. However, the frequencies of the oscillations and the decay time were very different for the two axes. There is little similarity in the 1 cycle signals, whereas the 10 cycle signals shows reasonably good similarity. Figure 3.13 shows the outputs of

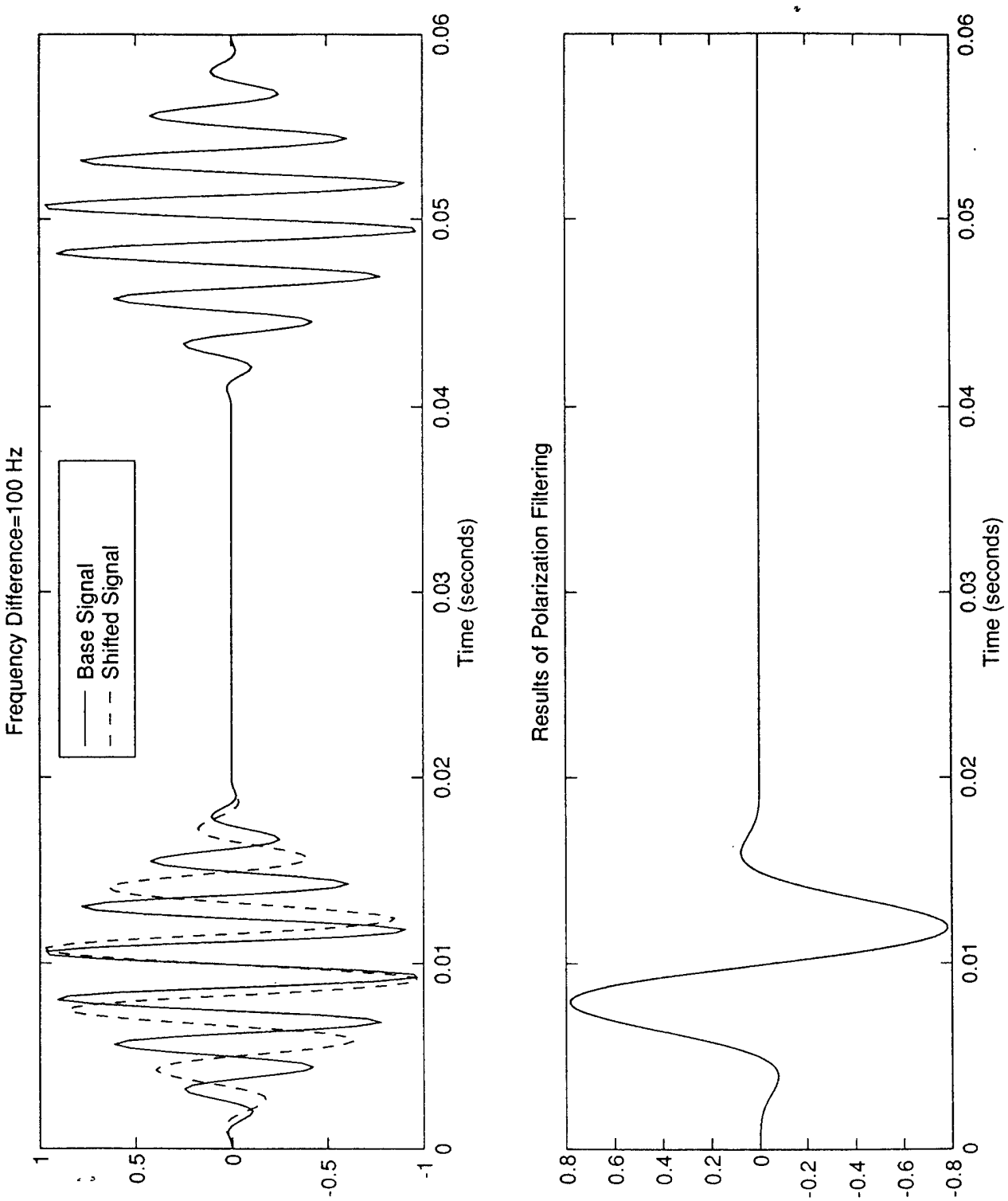

Figure 3.10. Same as Fig. 3.8 except the signals in the first pulse (top) have different frequencies rather than different phases. The output of the polarization filter (bottom) is bipolar in this case.

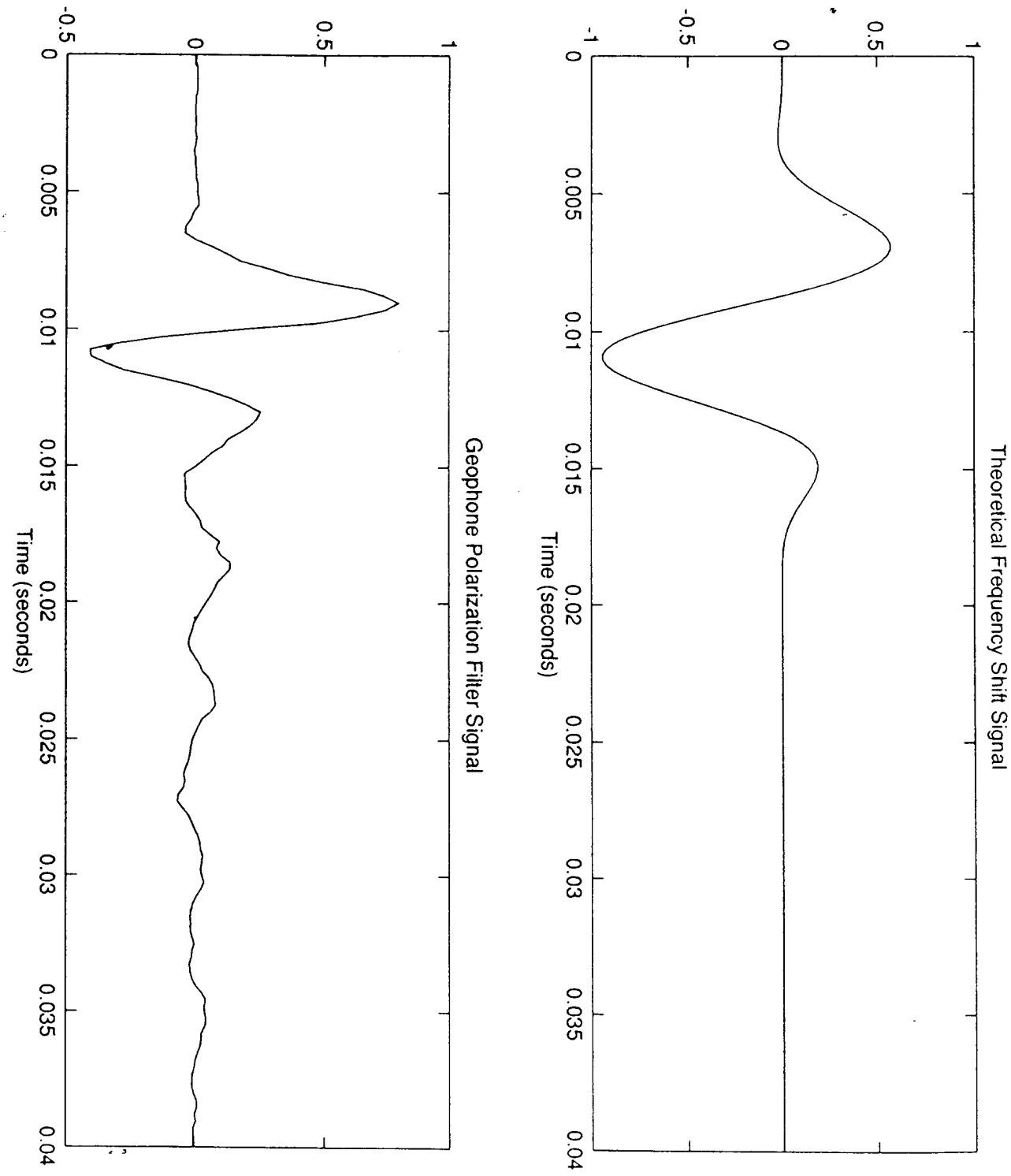

Figure 3.11. Comparison of the simulated output of the polarization filter from Fig. 3.10 (top) to that from the real data (bottom).

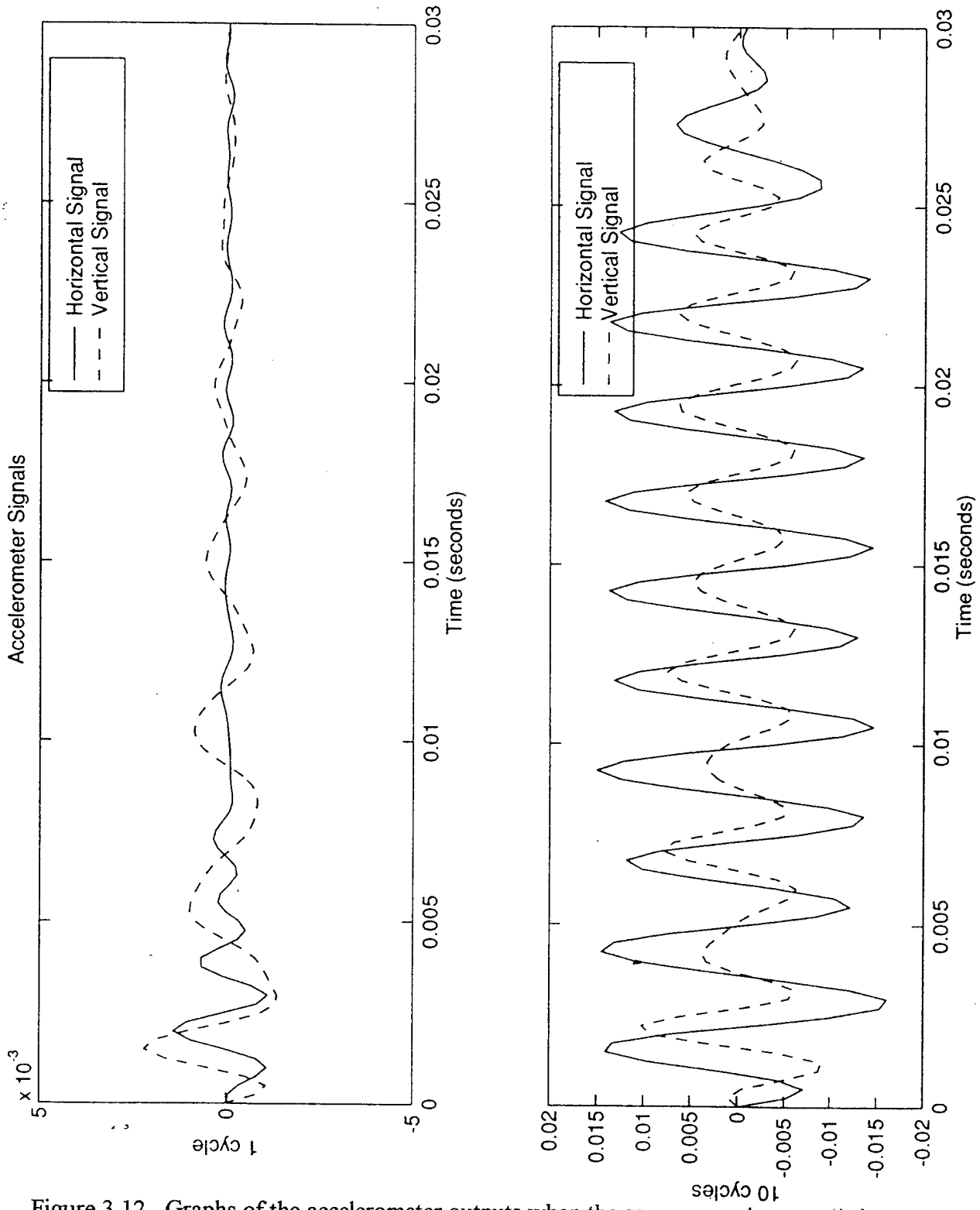

Figure 3.12. Graphs of the accelerometer outputs when the source was driven with 1 cycle (top) and 10 cycles (bottom). simulated output of the polarization filter from Fig. 3.10 (top) to that from the real data (bottom).

geophones for the same drive conditions as in Fig. 3.12. One notable difference is in the 1 cycle data. The horizontal geophone signal lasts much longer than the foot motion. The reason for this difference was not clear. It might indicate either a reverberant environment, or resonance(s) in the source mounting beam, the source connecting rods, or the speakers. Figures 3.14 and 3.15 show the power spectral densities of the horizontal 1 cycle and 10 cycle geophone signals. Figure 3.14 shows the vertical data, Fig. 3.15 the horizontal data. The main conclusion is that given a sufficiently long input signal, the source will produce the same frequencies in both axes.

For signals of approximately 10 cycles or more, or approximately steady-state conditions, the response was closer to the excitation frequency (which was 400 Hz in this case). In short, to have a predictable transmission to the sand, the excitation signals' pulse period must approximate steady state conditions in the source. However, assuming a propagation speed of 100 m/s, the wavelength at 400 Hz is 25 cm. Therefore, the length of a 10 cycle pulse is 2.5 m, which is comparable to the dimensions of the test tank. The conclusion to be drawn is that the test tank was too small to perform an adequate investigation of surface waves.

These results were further complicated by the following: assuming an average group speed range between 50 m/sec and 100 m/sec and a minimum of 10 cycles per pulse, choosing the worst cases, the wavelengths of the source signals could range from 2.5 to .5 meters in space. These wavelengths are too large to resolve any features in the tank. Specifically, polarization analysis, or any algorithm that required frequency stability,

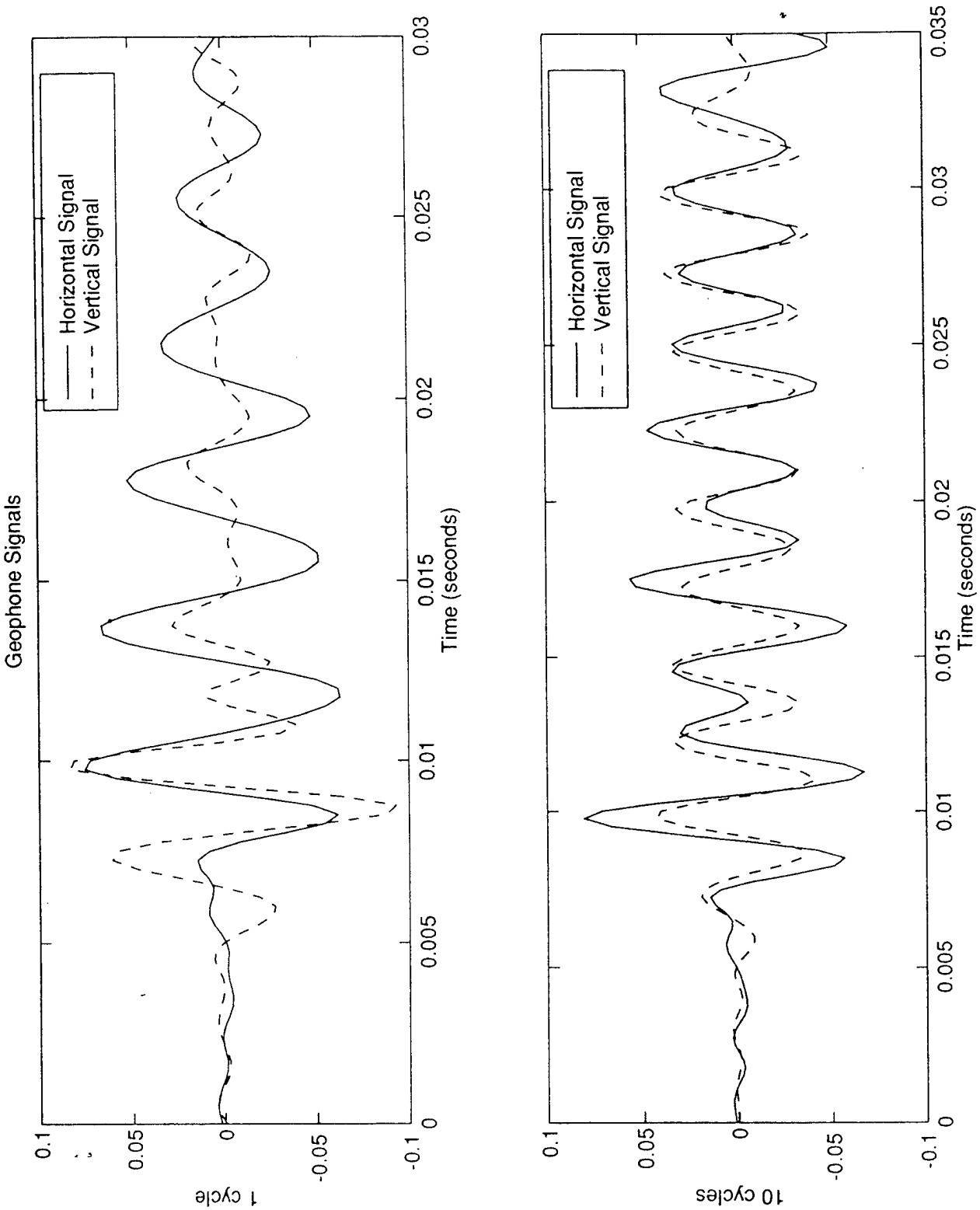

Figure 3.13. Graphs showing the output of the geophone for the same conditions as in Fig. 3.12.

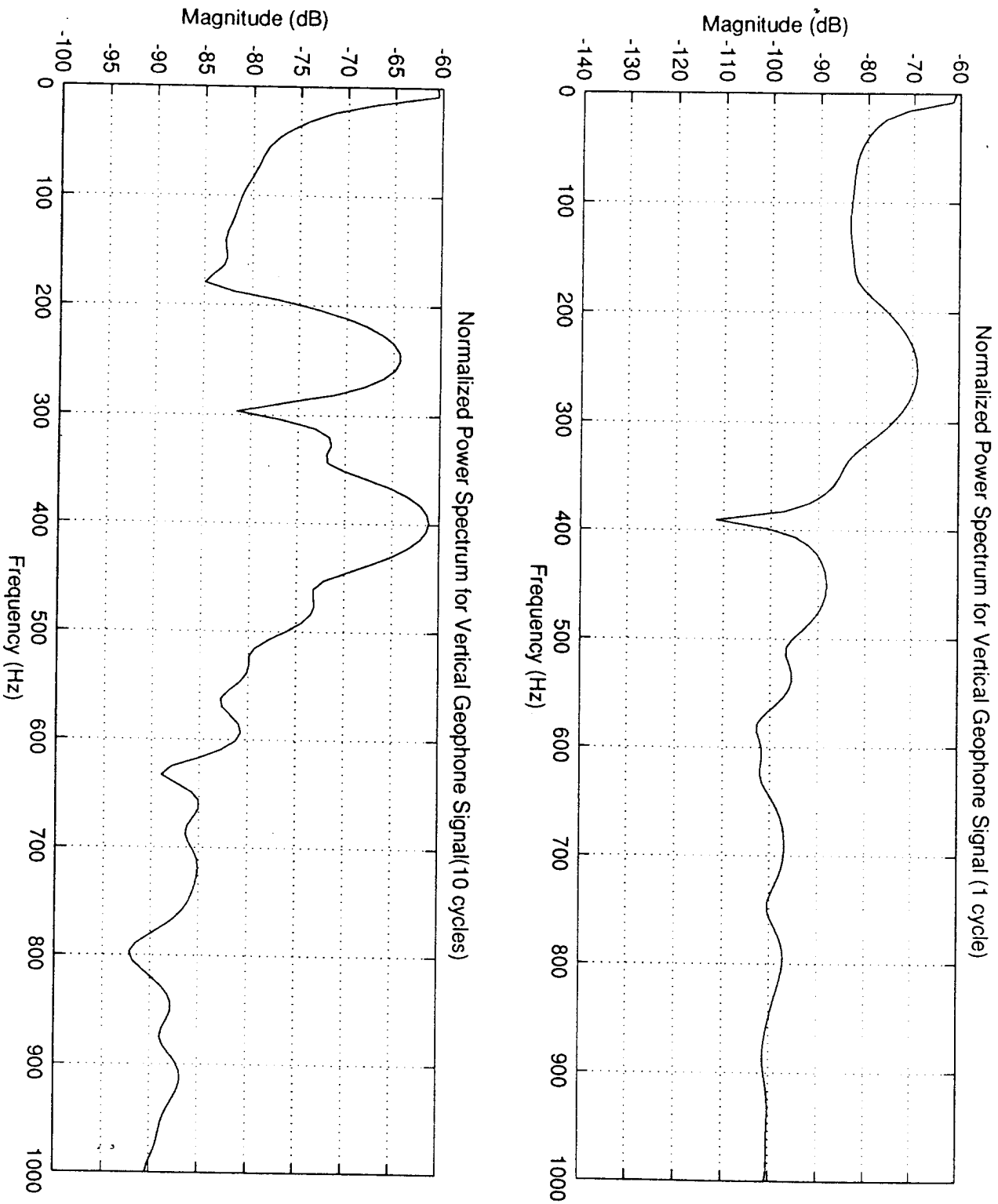

Figure 3.14. Graphs of the power spectral density of the vertical geophone output when the source is driven with 1 cycle (top) and 10 cycles (bottom).

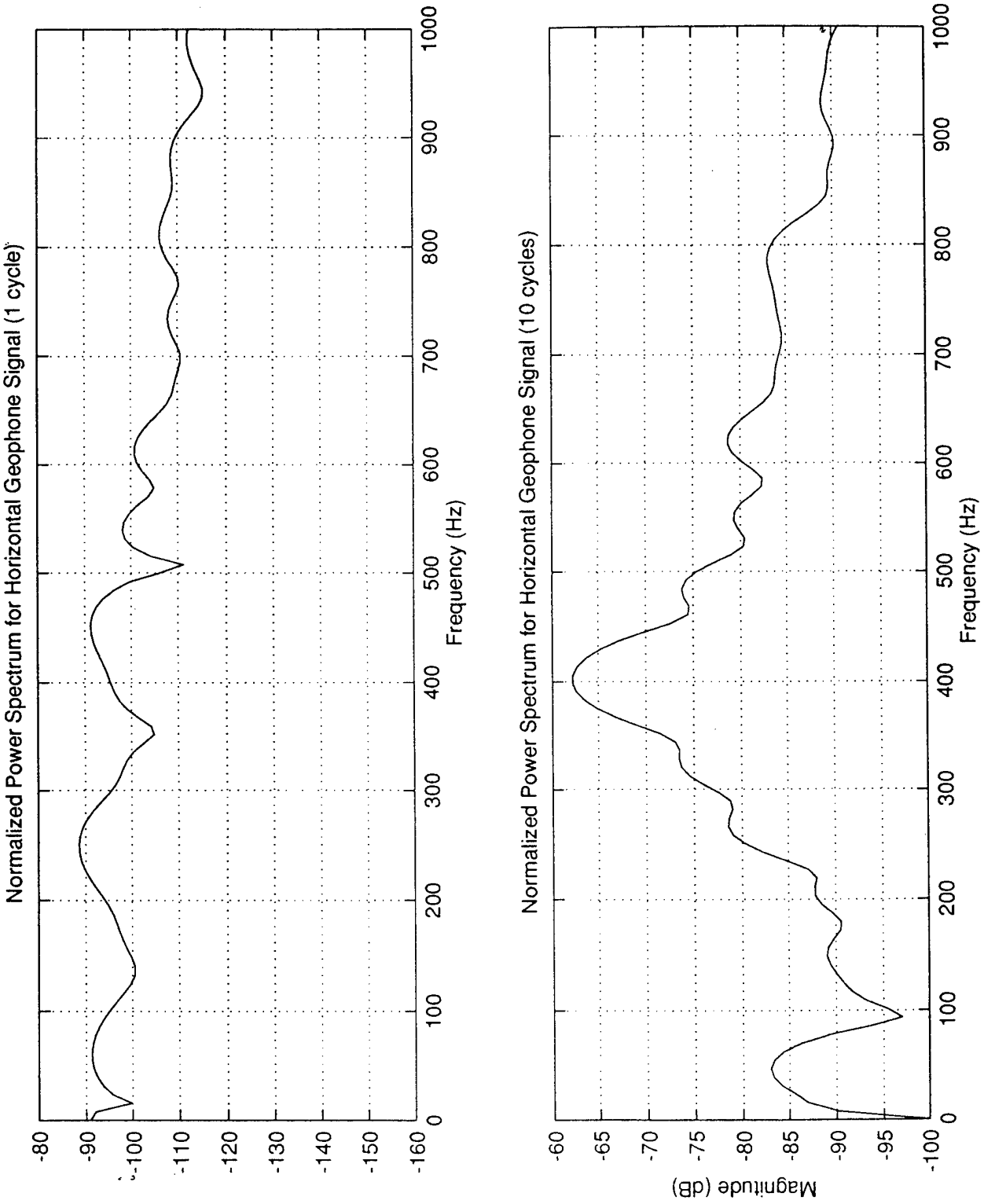

Figure 3.15. Same as Fig. 3.14 except for the horizontal geophone.

could not be utilized with this two-axis design in this test tank. The same analysis was performed on signals excited by the single-axis source with similar results.

IV. SCATTERING EXPERIMENTS

A. COMPARISON OF SINGLE-AXIS AND TWO-AXIS SOURCE SCATTERING EXPERIMENTS

This chapter contains results of a series of scattering measurements. The target was a 61 cm x 6 cm x 2 cm brass plate. In the first series of measurements, the two-axis source was located 100 cm from the left side of the tank. The two-axis geophone was located 30 cm colinear and to the right of the source along a diameter of the tank (see Fig. 4.1). The source was excited with a single cycle at 400 Hz. The phase difference between the two sources was 90^0.

First a background reading was recorded. Then the target was buried 85 cm from the source with its largest cross section facing the source-receiver. Its top edge was flush with the sand's surface. So as viewed from the receiver the target was 61 cm wide and 6 cm high. It took approximately 4 to 7 minutes to take the background signal, bury the target and then take the second reading. The results are presented in Fig. 4.2. The upper figure shows the vertical signal, the lower figure the horizontal signal. The vertical background signal shows two prominent features: one pulse lasting from approximately 0.005 to 0.0235 and another from approximately 0.024 to 0.038 s. The signal with the target present was very similar. The only significant difference occurred at approximately 0.02-0.027 s. Upon closer inspection, the two traces began to differ at about 0.015 s.

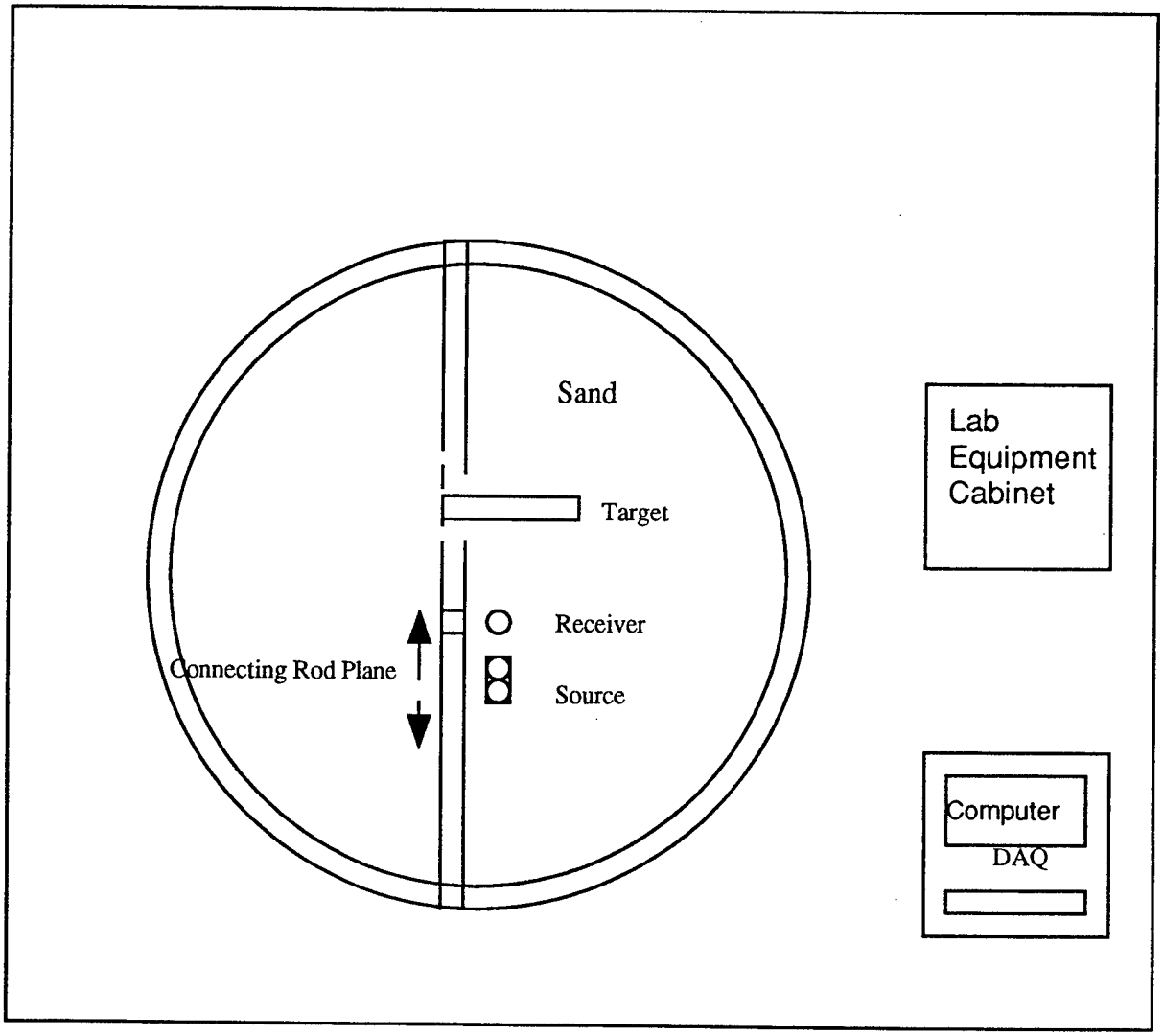

Figure 4.1. Top view showing the relative source, receiver and target alignment during data acquisition.

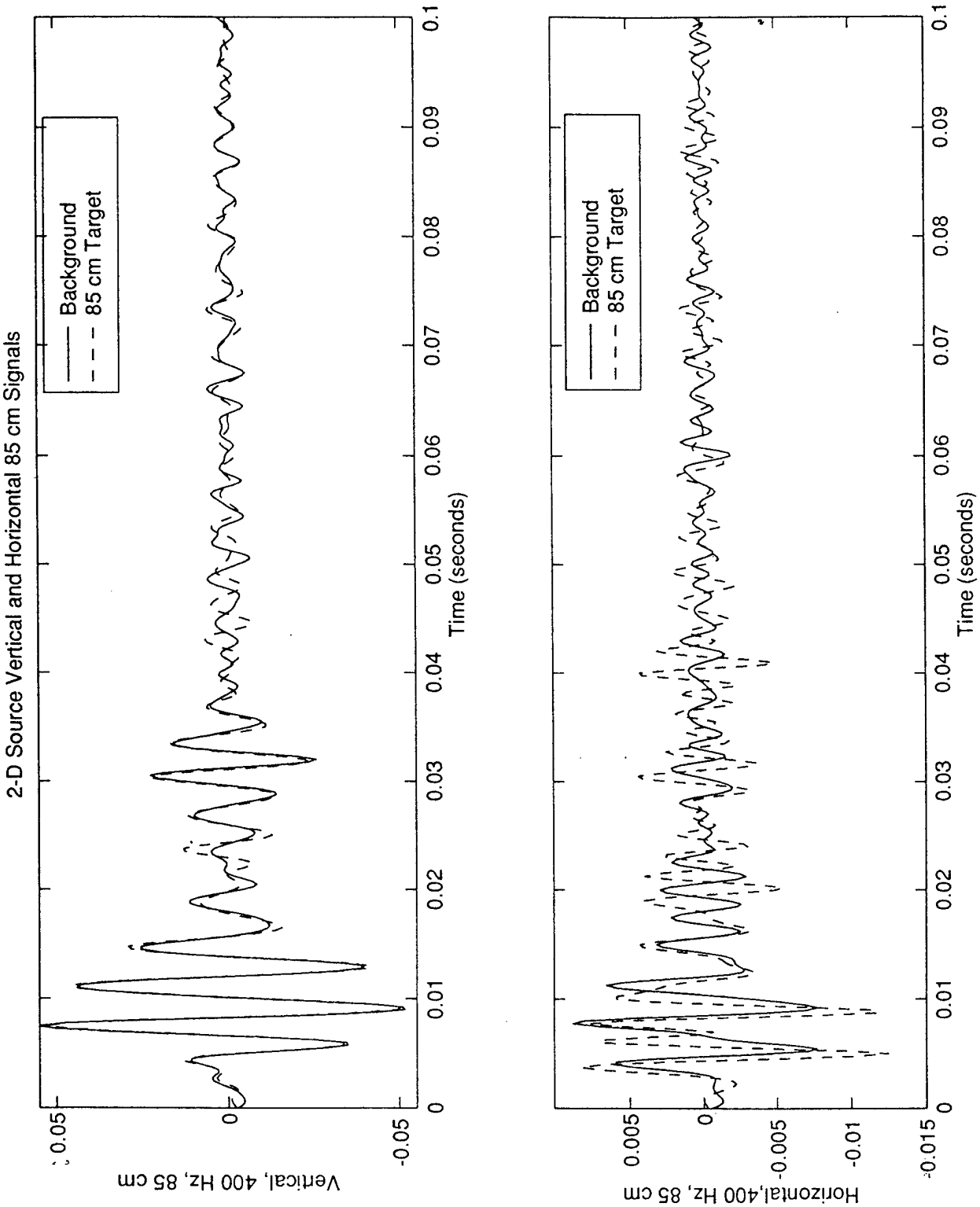

Figure 4.2. Graph showing the output of the geophone with (dashed) and without (solid) the target present. The target range was 85 cm from the source foot. The two-axis source was driven with a single 400 Hz cycle

There was another, much weaker discrepancy at approximately 0.035-0.05s. This data therefore might indicate that the return from the target arrived at the receiver at about 0.015s after transmission. The complete path distance was approximately 140 cm, so the propagation speed was approximately 90 m/s. The origin of the second pulse in the background and scattered signals is not known.

The horizontal signal behaves very differently. The background and scattered signals are different right from the start. There is evidence of many more echoes or multipath arrivals than with the vertical signal. The horizontal signal does not lend itself to as simple analysis as the vertical signal.

The measurements were repeated with the target 60 cm from the source. The signals are shown in Fig. 4.3. The vertical signal is similar to that in Fig. 4.2, except the discrepancy between background and scattered signals begins earlier, consistent with a shorter path length. The horizontal signal is also similar to that in Fig. 4.2. It is equally different than the vertical signal and equally difficult to interpret.

The measurements were repeated with the one-axis source from Ref. 1. The signals are shown in Figs. 4.4 and 4.5 for 85 cm and 60 cm target distances, respectively. The total time required to complete the two-axis and single-axis experiments was approximately 12 minutes. The background signals for the one and two-axis sources are roughly the same. The main difference was that the second pulse in the vertical signal was

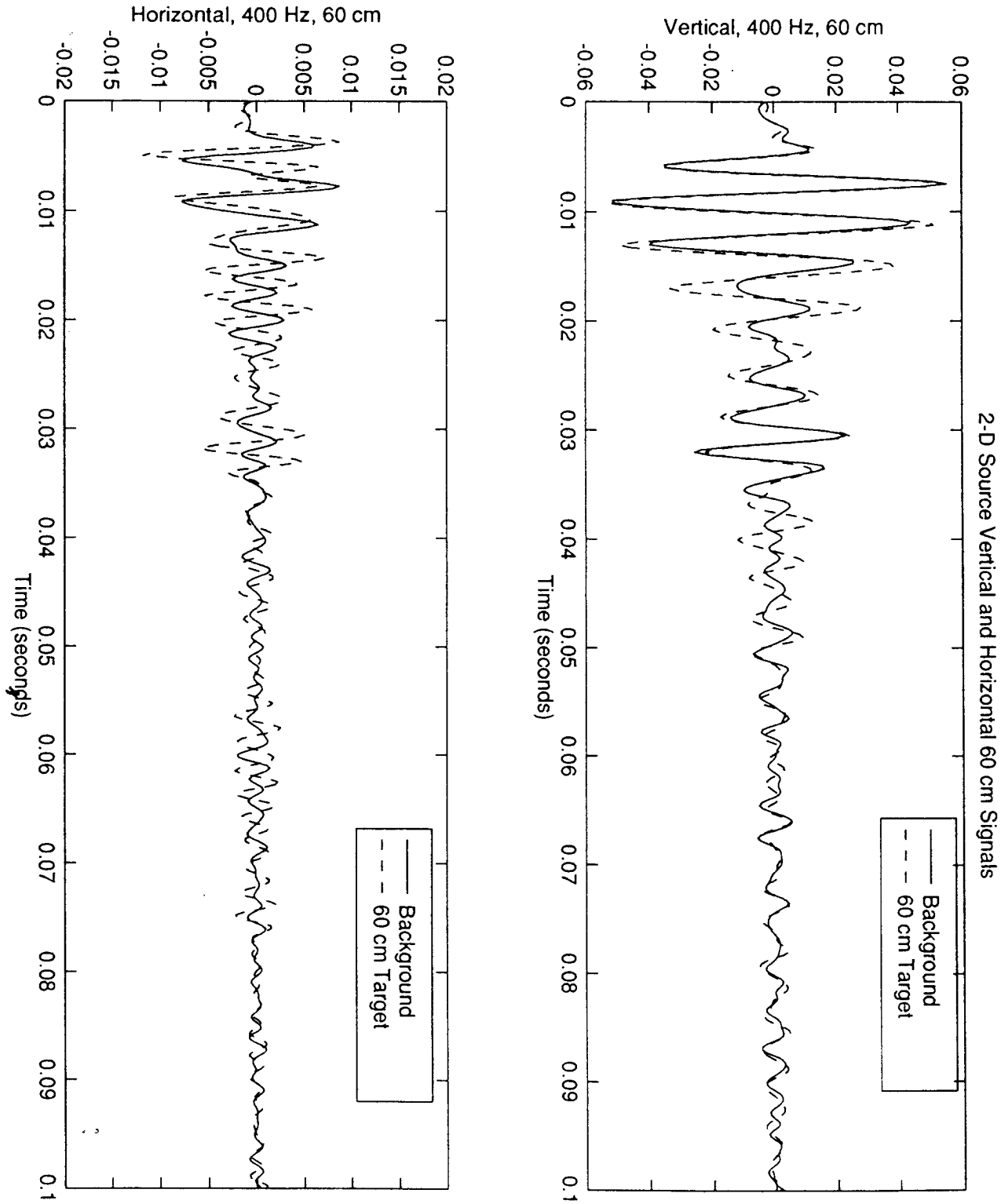

Figure 4.3. Same as Fig. 4.2 except for a 60 cm target range.

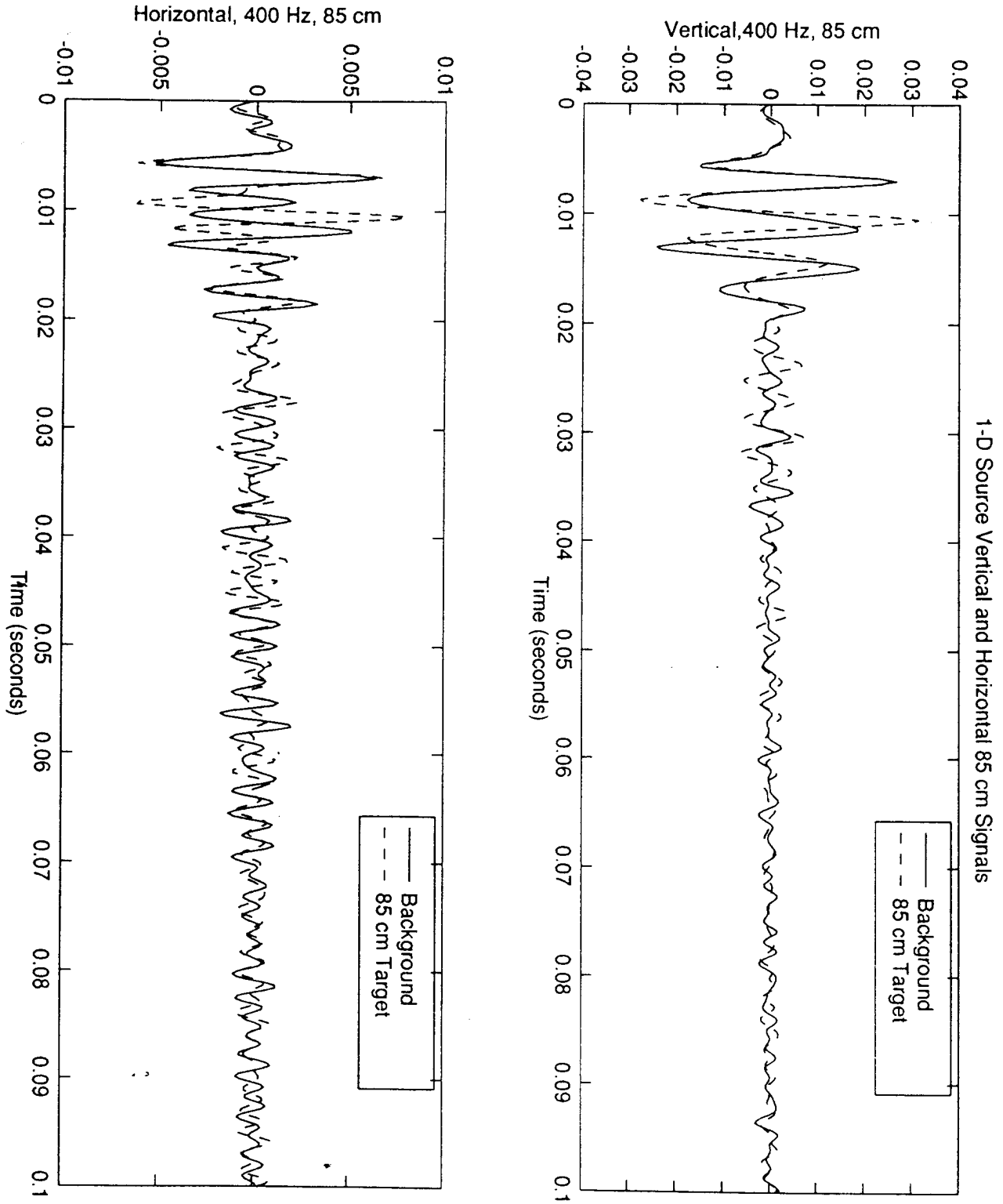

Figure 4.4. Same as Fig. 4.2 except the source was the single axis source.

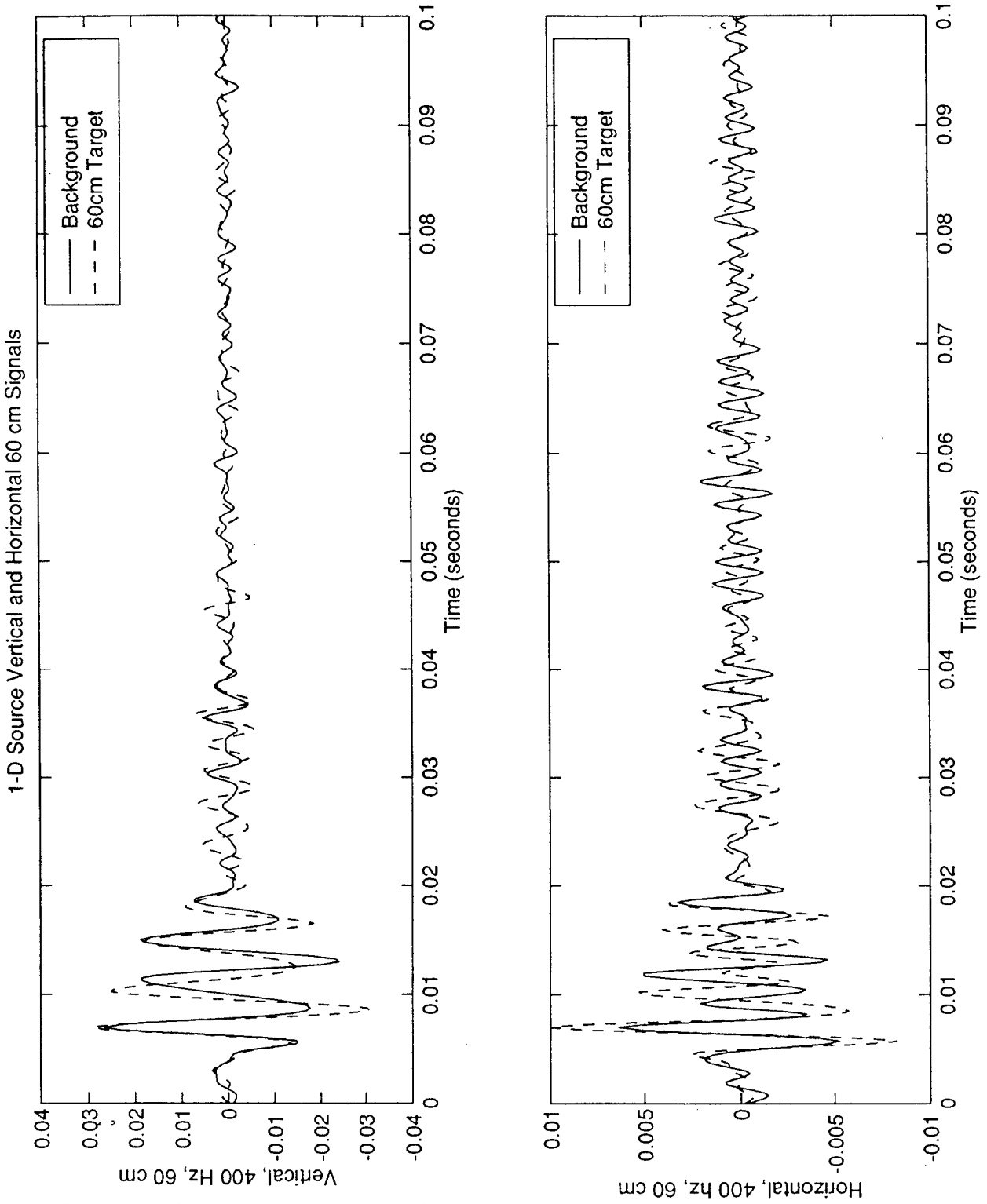

Figure 4.5. Same as Fig. 4.3 except the source was the single axis source.

weaker with the one-axis source. It was surprising that the vertical signals with the target present were very similar. The identification of a feature that arrives earlier with the 60 cm target than the 85 cm target is not obvious. Again the horizontal signals are different from the vertical signals. Unfortunately, they are also difficult to interpret.

The main conclusion from these measurements is that is that the information in the vertical and horizontal signals was different. Conducting these measurements in a more free-field environment may yield more easily interpreted signals. Further, use of the information in both axis may perhaps lead to identification of surface wave components in the signals.

Other methods used to extract the target from the received obstructed signals included subtracting the obstructed and background signals. This process sometimes yielded a definite pulse that correlated to the buried object. However, most times, this process did not yield any useful information. This inconsistency was attributed to the theory that the propagation was dominated by reverberation. Ref. 2 documents the effects of small changes in sediment particle size and the resulting interface that can make subsequent target detection difficult. It is not unreasonable to apply this theory to this test environment. Specifically, this test tank's sides and bottom can be assumed to model rigid interfaces which can support many reflections and the resultant noise field can make isolation of the target reflection difficult. These reverberation effects become more evident when using analysis techniques designed to separate and identify reflections in acoustic propagation. This will be further described in the next section, Cepstrum Analysis.

B. CEPSTRUM ANALYSIS

Autocorrelation and autospectrum analysis may identify the presence of two paths and the difference in their propagation times from the source to the geophone. When two or three paths are present, however, the identification of individual paths becomes more difficult [Ref. 4]. A Fourier transform of the output spectrum (called the cepstrum) will convert the individual interference components into more readily identifiable cepstral peaks at frequencies corresponding to $\Delta f\_ik = 1/|\tau_i-\tau_k|$, $i \neq k = 1,2,3,$ . . ., r [Ref. 4]. Specifically,

$$c_x = 1/2\pi\int \log|X(e^{j\omega})|e^{j\omega n}\,d\omega \qquad (4.1)$$

is the real cepstrum of a signal x. $|X(e^{jw})|$ is the magnitude spectrum of the signal x. Thus c_x is the inverse Fourier transform of the logarithm of the magnitude spectrum of signal x.. The limits of integration range from $-\pi$ to π.

The following example is taken from Ref. 4 and demonstrates the potential of cepstrum analysis. A degraded sonar signal pulse

$$t*\exp^{-at} \qquad (4.2)$$

with damping coefficient a = 0.06, was degraded by adding a delayed, attenuated replica of the basic pulse. This data was input to the cepstrum algorithm. The results appear in Fig. 4.6. The upper trace in Fig. 4.6 shows the composite signal and the echo that was delayed 55 seconds relative to the basic waveform. This peak is easily seen in the lower trace of Fig. 4.6. Figures 4.7 through 4.10 show the results of cepstrum analysis applied to the scattering experiment data collected in section 4A. Each of these figures show the cepstrum of the background, target, and difference between the background and target signals. In general, the cepstrum plots show small amplitude features which do not correlate to any particular propagation path and the inherent difference between vertical and horizontal signals did not seem to have any effect on the resultant cepstrum signals. In each case, the cepstral signals followed the same form but did not show any clearly defined features that correlated to the target. The difference signals mirrored the target signals, but did not otherwise show any interesting features. The reasons for these results is not clear. They could be attributed to the reverberant field masking the potentially weak target feature (as described in Ref. 2) or a modal feature of the tank that we do not understand.

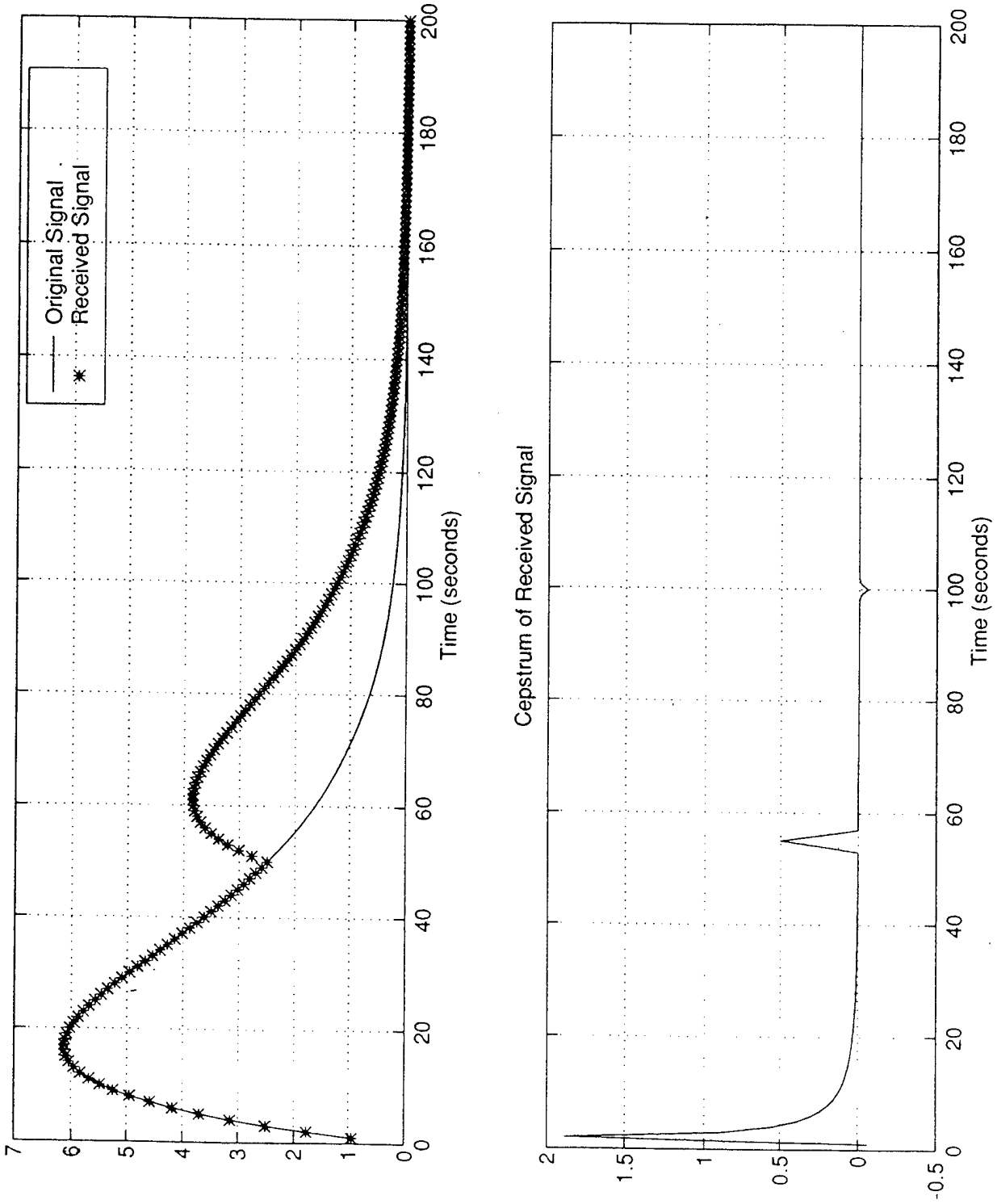

Figure 4.6. Graph showing the results of Cepstrum analysis (bottom) of the signal indicated by the * in the top figure.

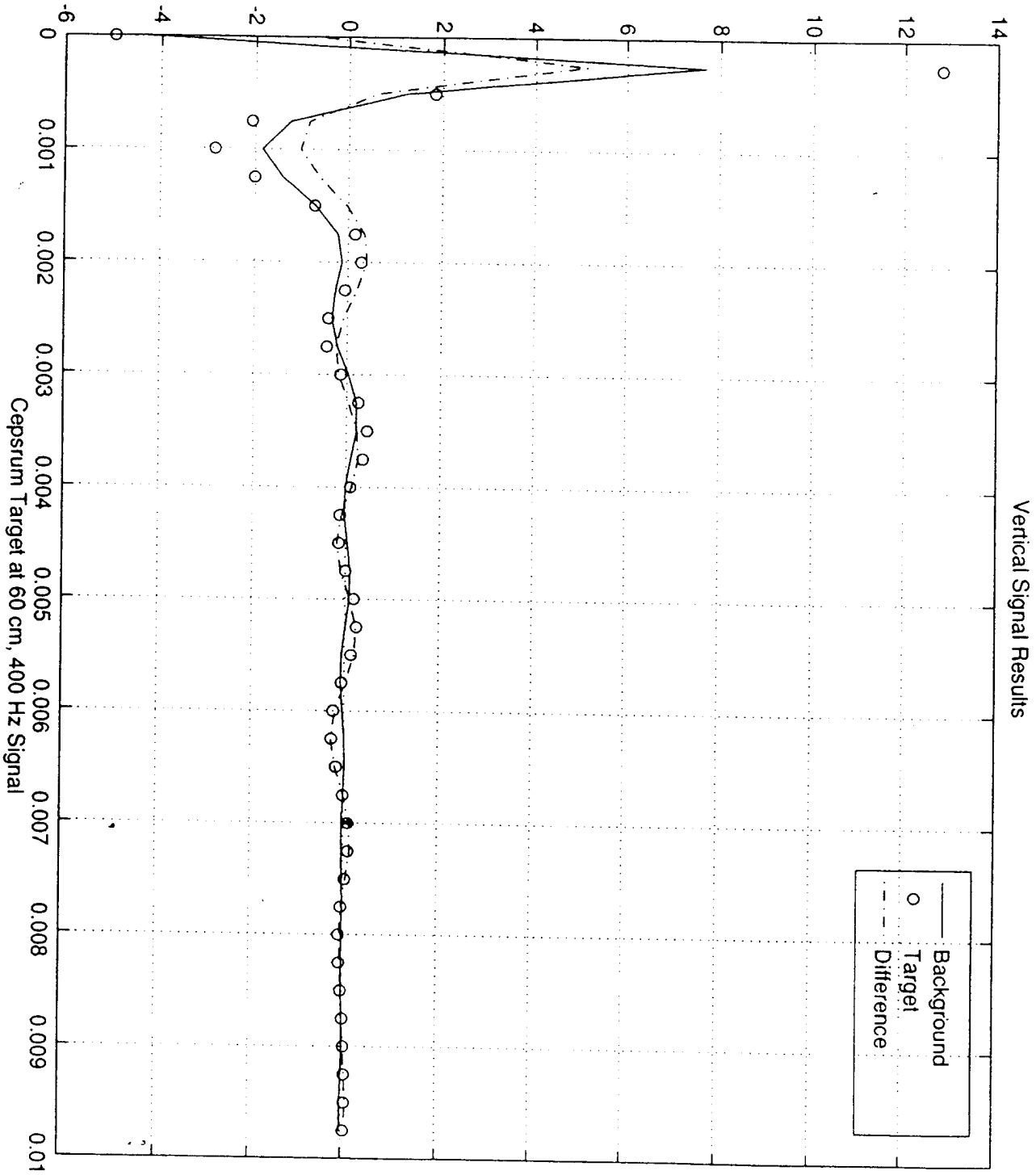

Figure 4.7. Results of Cepstrum analysis of the vertical signal data shown in Fig. 4.3. The dashed line indicates the difference in the Cepstrum of the background and with the target signals.

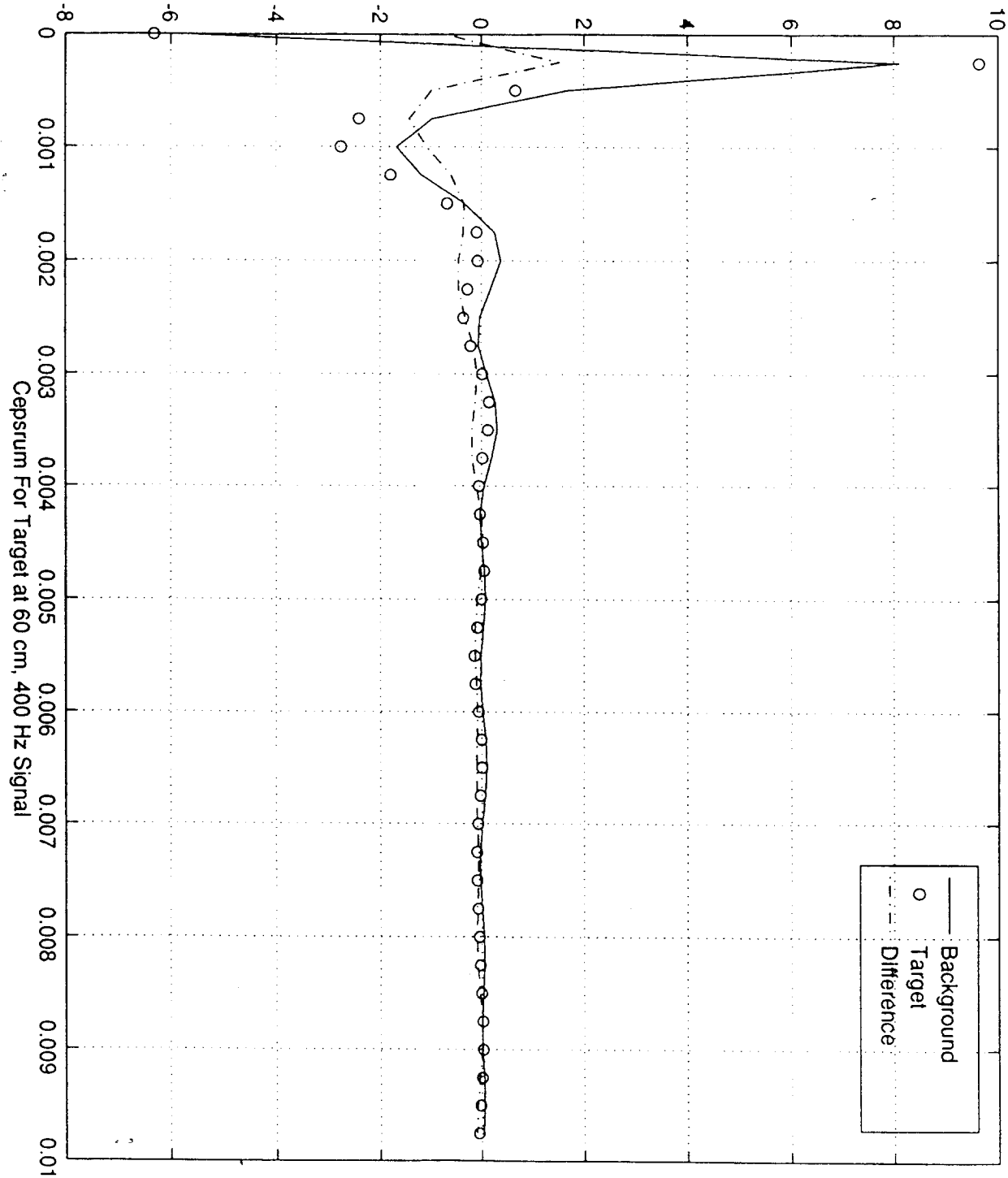

Figure 4.8. Same as Fig. 4.7, except the data are from the horizontal geophone.

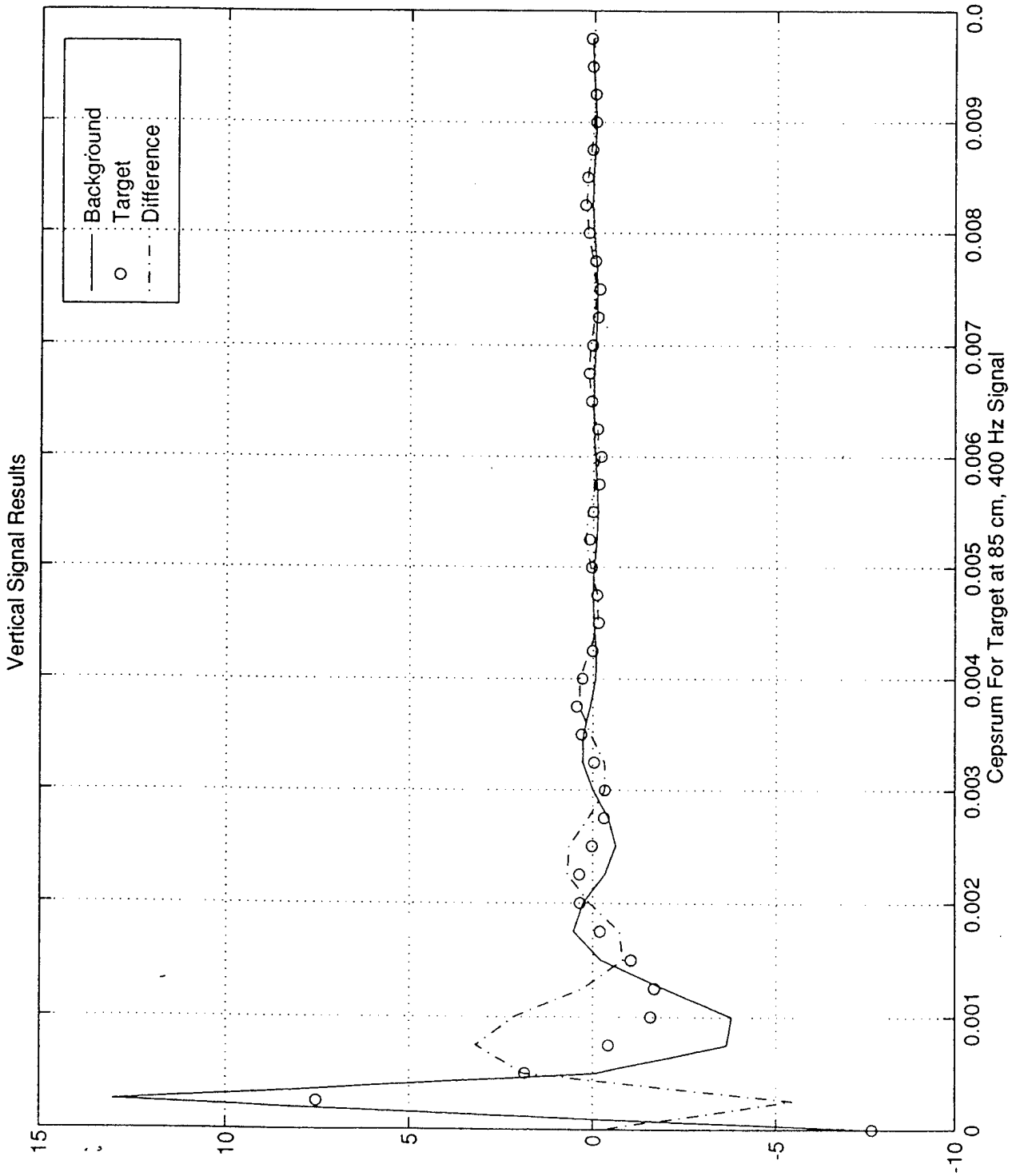

Figure 4.9. Same as Fig. 4.7, except the data are the vertical signals from Fig. 4.4.

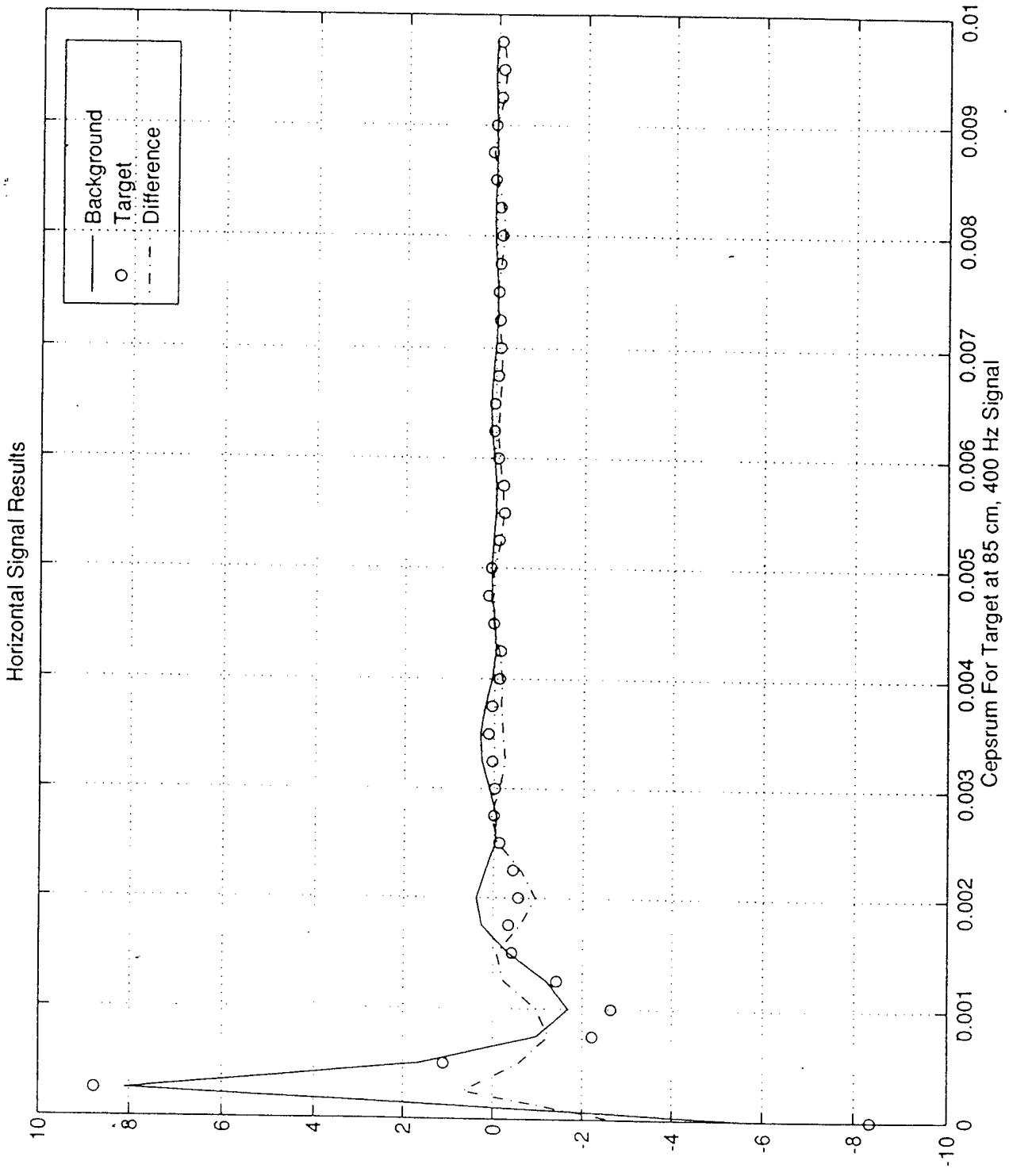

Figure 4.10. Same as Fig. 4.7, except the data are the horizontal signals from Fig. 4.5.

V. CONCLUSIONS AND RECOMMENDATIONS

This thesis describes the design and testing of a two-axis source and a two-axis receiver for use in buried object detection. The purpose of the two-axis source was to be able to selectively excite surface waves in water-saturated sand, exploiting the elliptical particle motion. The purpose of the two-axis receiver was to take advantage of the surface wave phasing to filter out signals from non-surface wave modes of propagation.

We successfully demonstrated the ability to generate particle motions with different phasing with the source. Definitive demonstration of surface wave generation was not possible, however, because of limitations imposed by due the size of the test tank. Long pulses caused reverberation problems. Single cycle excitation resulted in different frequency and phase contents in vertical and horizontal signals, ruling out the possibility of detecting constant phase differences.

Scattering experiments demonstrated the advantage of a two-axis receiver. The information content in the two channels were unexpectedly different. The main recommendation is to test the system on a beach to more closely approximate free-field conditions.

APPENDIX A. LABVIEW VI FOR DATA ACQUISITION

One vi was used to acquire data. The vi is designed to be triggered by the HP 3314A Function Generator. The vi should acquire a specific number of received waveforms from each channel and average them. The three programming elements required were a "for loop," shift registers and an intermediate vi call AI wave. The three elements can be seen in the simplified version shown in Fig. (A.1). The book icon is a "for loop." The arrows on each side are shift registers. In this case the "for loop" value is 100. Therefore, 100 acquisitions are made, summed and then divided by the "for loop" value to get an average of the signal. This is timed and buffered acquisition. This means that the hardware clock is used to control the acquisition rate and the data is stored in an intermediate memory buffer after it is acquired from the input channel. Figure (A.2) shows the elements of the actual vi. The left side of Fig. (A.2) shows the front panel inputs controlling the number of iterations, number of channel inputs, specific device, trigger type, and scan rate information. Figure (A.3) shows the actual front panel.

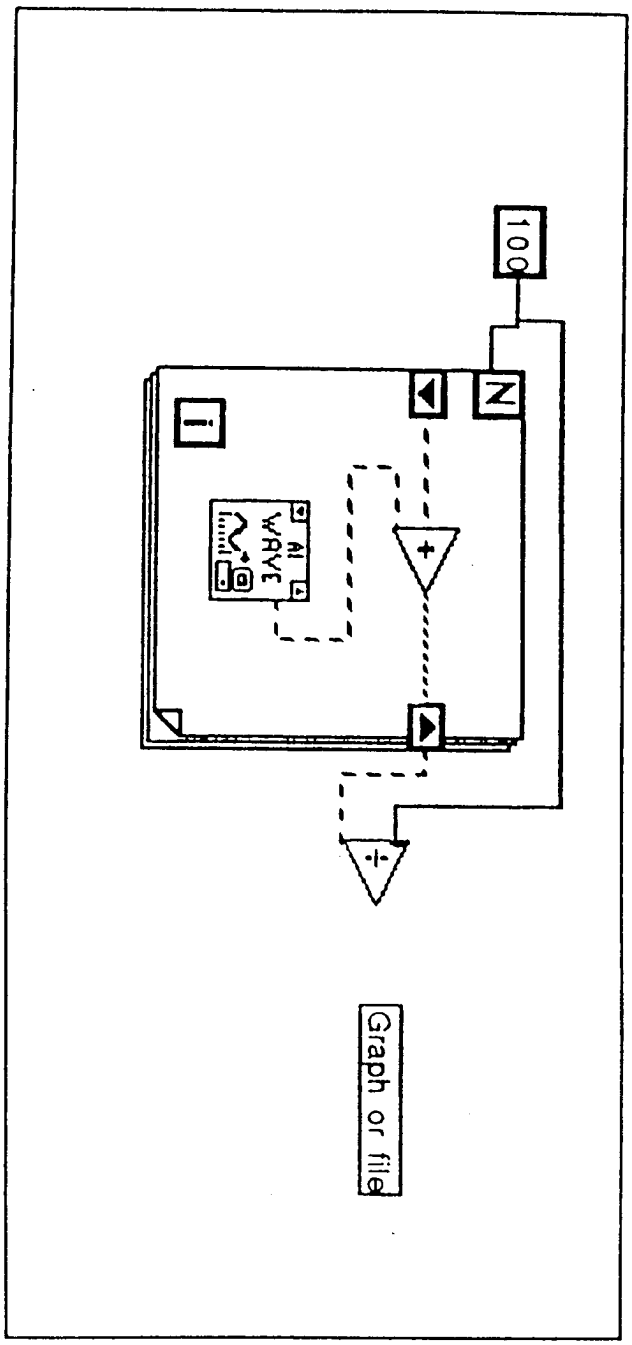

Figure (A.1). Elements of Data Acquisition.

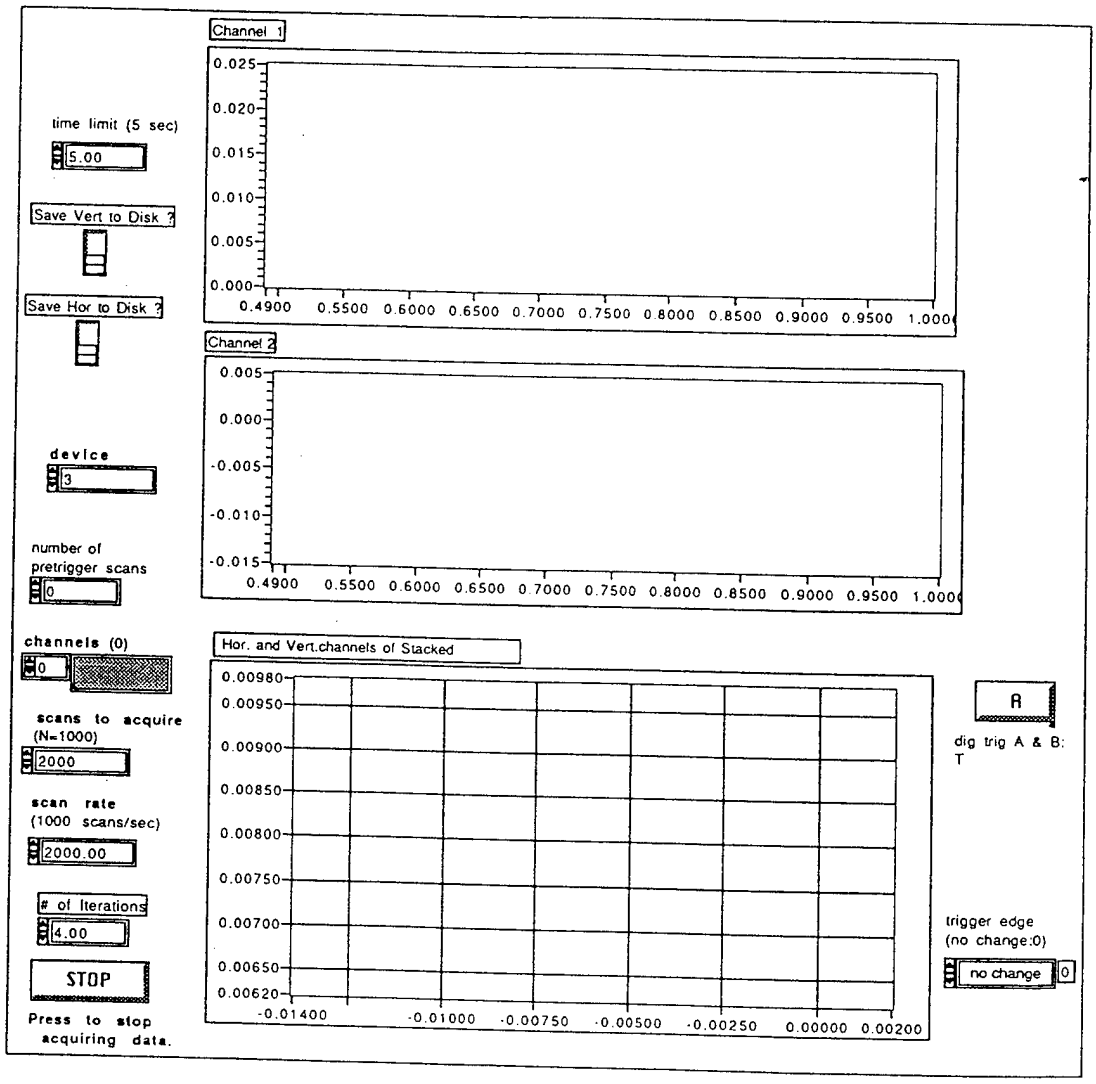

Figure (A.2) Data Acquisition vi front panel.

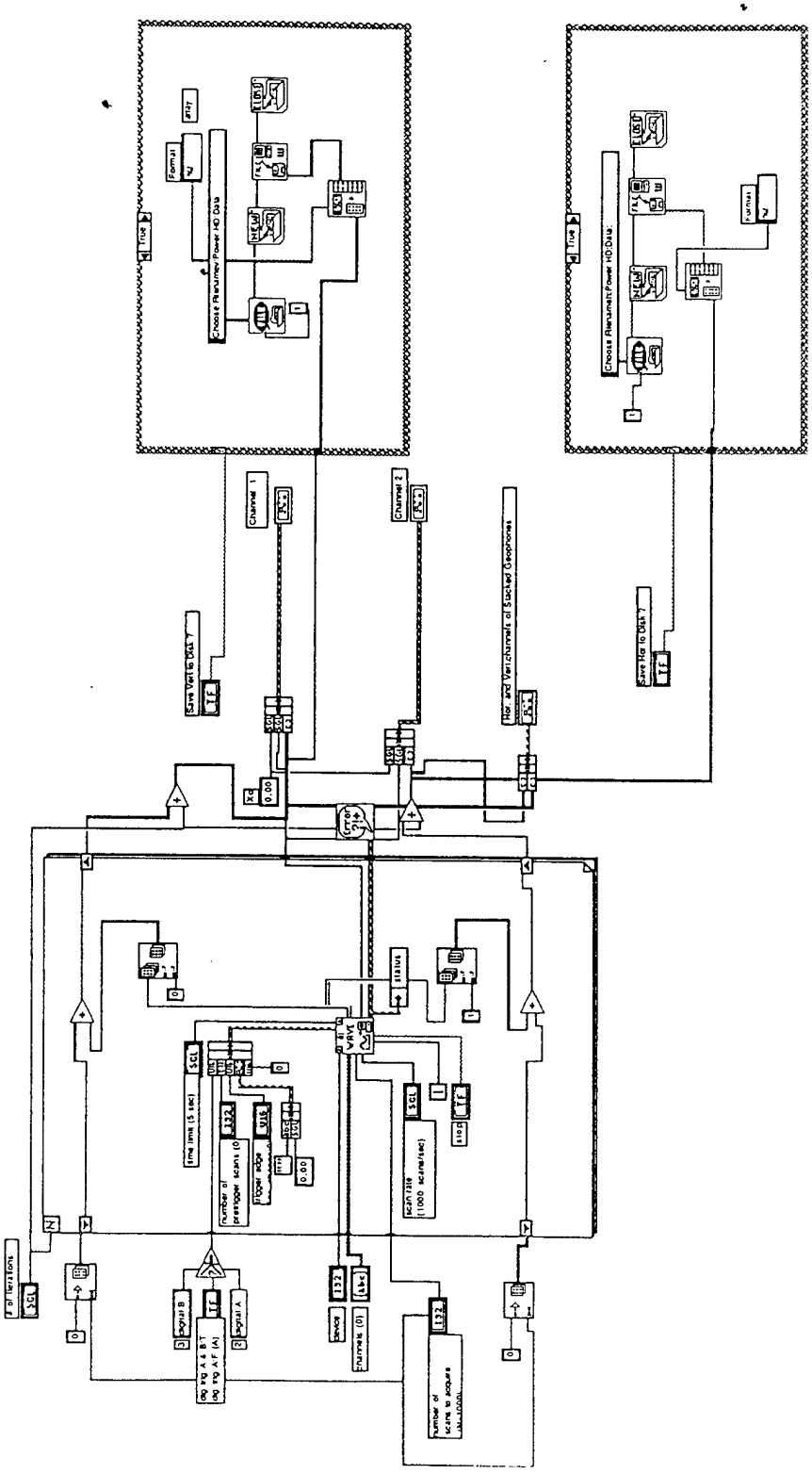

Figure (A.3). LABVIEW vi for data acquisition.

APPENDIX B: FACT SHEET FOR GEOPHONES

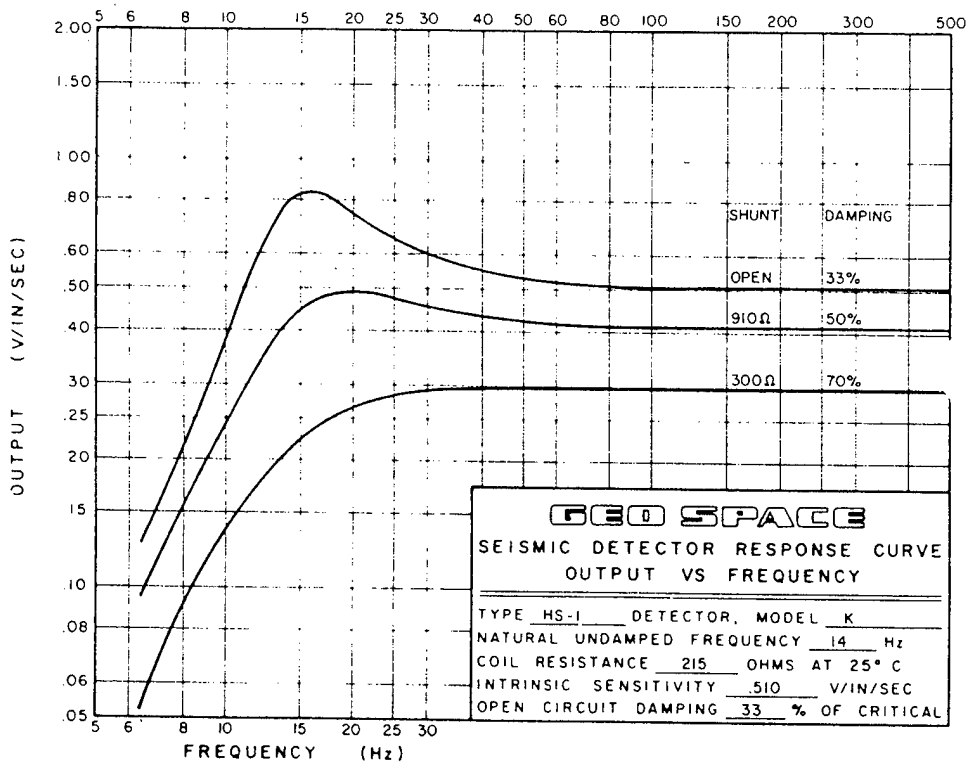

Figure (B.1). Fact sheet for geophones.

APPENDIX C: FACT SHEET FOR SOURCE ELEMENTS

WOOFER SPEAKER

4"(10cm) Woofer

Cat. No. 40-1022B

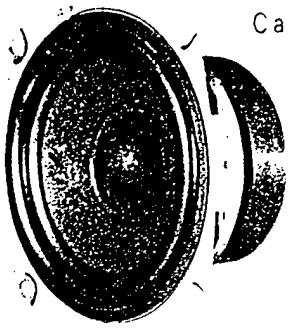

FEATURES

- Smooth frequency response
- Light weight hard cone paper based on careful study of internal loss values
- Uprolled rubber edge minimizes distortion and improves linearity
- Long travel voice coil for high power handling

SPECIFICATIONS

Impedance	8 ohms
Frequency response	50 - 7,000Hz
Free air resonance	55Hz + 5Hz
Qts	0.35
Vas	0.23 cft
Vas is the volume of air that is acoustically equivalent to the compliance of the cone	
SPL	84 + 2dB/W (1m)
Input power nominal)	5W
Input power (maximum)	10W
Magnet weight	228 g 8.0 oz
Speaker	700 g 24.7 oz

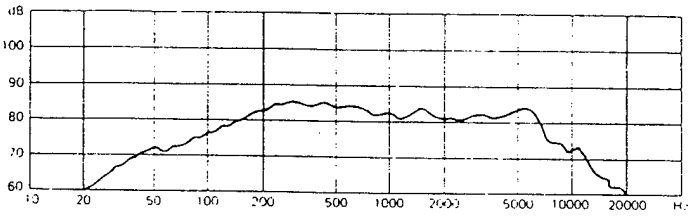

HOW TO USE

1. Installation:
   a. Install the woofer unit from the enclosure front and keep it flush with the baffle surface
   b. Secure the speaker so that no air leakage is permitted.
2. Connections-when using with a tweeter in a two-way system connect as shown

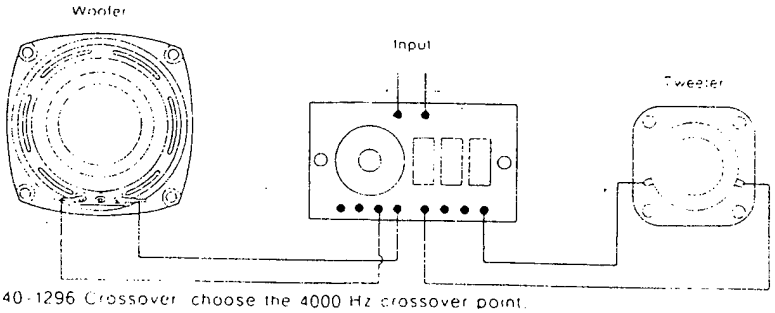

Note: When using the 40-1296 Crossover choose the 4000 Hz crossover point.

Figure (B.1) Fact Sheet for geophones.

REFERENCES

1. Stewart, W., "Buried Object Detection Using Surface Waves," Master's Thesis Naval Postgraduate School, 1995.

2. Smith, E, et al, "Measurement and Localization of Interface Wave Reflections from a Buried Object," J. Acoust. Soc. Vol 99(4), 2499 (A),1996 .

3. Johnson, G. H., "Labview Graphical Programming," McGraw-Hill Inc., 1994.

4. Childers, D. G., and Kemerait R. C., "Signal Detection and Extraction by Cepstrum Techniques," Proc. IEEE, vol. 57, 1972.

INITIAL DISTRIBUTION LIST

1. Defense Technical Information Center.....2
   8725 John J. Kingman Rd., STE 0944
   Ft. Belvoir, Va 22060-6218

2. Dudley Knox Library.....2
   Naval Postgraduate School
   411 Dyer Rd.
   Monterey, California 93943-5101

3. Anthony A. Atchley.....5
   Code PH/Ay
   Naval Postgraduate School
   Monterey, California 93943-5101

4. Donald L. Walters.....2
   Code PH/We
   Naval Postgraduate School
   Monterey, California 93943-5101

5. Department of Physics.....1
   Code PH
   Naval Postgraduate School
   Monterey, California 93943-5101

6. Anthony J. Anglin.....2
   90 Glen Lake Drive
   Pacific Grove, California 93950